UNITED NATIONS UNIVERSITY
GEOTHERMAL TRAINING PROGRAMME
Orkustofnun, Grensásvegur 9,
IS-108 Reykjavík, Iceland

Reports 2008
Number 26

GEOCHEMICAL INTERPRETATION OF THE MASAYA-GRANADA-NANDAIME CHEMICAL DATA, NICARAGUA

José Francisco Ruiz Cordero
Ministry for Energy and Mines
Department of Geothermal Energy
Managua
NICARAGUA C.A.
francisco.ruiz@mem.gob.ni

ABSTRACT

The available chemical data for the Masaya-Granada-Nandaime area have been evaluated applying HCO_3-Cl-SO_4 and Na-K-Mg ternary diagrams, geothermometry (silica and cation), isotopes, mixing models and speciation using the WATCH program. According to the HCO_3-Cl-SO_4 ternary diagram, only the water samples from Apoyo Lagoon and Granada City region show potential for a geothermal system, and also a possible region with high permeability. According to the Na-K-Mg ternary diagram, the water samples are possibly composed of a mixture of geothermal water and surface waters or plain surface waters. The temperatures predicted using silica and cation geothermometers are not in a good agreement, with the predicted silica temperatures always lower than the predicted cation temperatures. The results suggest the existence of a geothermal system with the Apoyo Lagoon region at its centre.

1. INTRODUCTION

1.1 Geothermal areas in Nicaragua

Nicaragua has an active volcanic cordillera that extends along the Pacific coast and is responsible for the occurrence of high-temperature areas. Many geothermal investigations have been carried out in this area. These investigations began at the end of the sixties and were intensified after 1973, when a worldwide oil crisis impacted negatively on Nicaragua´s economy.

Geochemical, geophysical, hydrological and volcanological research was carried out in these areas. These investigations were reviewed in the Nicaragua Geothermal Master Plan carried out in the year 2000. The results of these studies made it possible to establish the existence of 10 geothermal areas (Figure 1), each of which has enough potential to be considered a feasible

FIGURE 1: Geothermal areas in Nicaragua

project. Some of the areas are eponymous with the volcanoes that were related to or responsible for the geothermal systems (CNE, 2001). The chemical data for the samples evaluated in this study can be seen in Tables 1-3 in Appendix I.

1.2 Brief description of the area

The Masaya-Granada-Nandaime area is located at the northwest end of Lake Nicaragua (Cocibolca) and comprises the entire region between the eponymous cities. The area under study has been selected taking into consideration the entire sector in which recent volcanism has taken place, as wellas extensive areas to the southwest and the north. Taking into account previous research and fieldwork carried out as part of the master plan, the study area is at least 1,100 km^2.

The Masaya, Apoyo and Mombacho volcanoes are aligned in a NW-SE direction in the area's central part. The Masaya caldera is located to the northwest side, Apoyo caldera is at the centre and the Mombacho volcano is to the southeast of the area. The Masaya and Mombacho structures are only 12 km apart and it can therefore be speculated that an important heat source may exist along the entire volcanic axis.

The Masaya volcanic complex, located in the extreme northwestern part of the study area, has formed an 11 km-long and 6 km-wide caldera with the Masaya Lagoon at its southeast end. The Apoyo caldera is a collapsed volcanic structure of 6-7 km in diameter, formed after a series of eruptions. At the bottom of this 350 m deep depression the Apoyo Lagoon is found.

The area has a tropical climate. The mean annual rainfall ranges from 1200 to 1300 mm. The greatest amount of rain occurs during the frequently irregular wet season. The mean annual temperature varies from 27.5ºC in the lowest zones between Masaya and Granada to about 25ºC around Apoyo Lagoon (INETER, 1997). At the summit of Mombacho Volcano the climate is particularly cool and humid (CNE, 2001).

1.3 Geological features of the area

The Mombacho is a stratovolcano that reaches an altitude of 1344 m, intersected in a northeast – southwest direction by large ravines caused by rock slides, one of which created the Granada islets in Lake Nicaragua which is next to the volcano on its east side. Its crater on the south side is open due to an immense landslide that spread lava blocks and detritus on its slope and flatland further to the south. This landslide covered an area of more than 40 km^2 and created several lagoons such as Juan Tallo, Verde, El Cacho and Blanca.

The area has been subject to volcanic processes dating from the Pliocene to recent times. Initial volcanism covered a very wide area with ignimbrite and agglomerate deposits, which reach a thickness of 250 m or more in some parts. Overlying these materials are a series of lavas and pyroclastic deposits of variable thickness, genetically associated with volcanism in the Masaya complex, the Apoyo caldera and the Mombacho volcano.

The Masaya complex, which occupies the area's northwest sector, is a composite volcanic centre of basaltic lavas and pyroclastic deposits. The volcano is affected by the caldera collapse resulting from a powerful explosive eruption that occurred a few thousand years ago. It is said that of all the volcanoes in Central America, Masaya has been the most active in historical time, and the intense activity of basaltic and basaltic-andesitic deposits scattered throughout the area seem to confirm this view.

The lagoon filled Apoyo caldera is an almost circular collapse structure. The lagoon walls rise to an altitude ranging from 100 m to 450 m. It is consistent with the collapse of a pre-caldera series composed of basaltic and andesitic lavas, and a pyroclastic series with intercalations of basaltic lavas. These originated after a series of eruptions catapulted dacitic pumice deposits, mainly to the east. Pre-caldera rocks have been dated at 100,000-360,000 years, while pyroclastic deposits associated with the caldera formation are between 23,000 and 21,000 year old. There are some rhyodacitic domes on the caldera's eastern and southern peripheries. One of them has been dated at 90,000 ± 40,000 years.

Mombacho is a stratovolcano of 50 km^3 in volume and reaching an elevation of 1,340 m. It is characterized by a series of lava flows, intercalated with pyroclastic products and two large rock slides that have truncated the volcano from the summit to the northeast and southeast. What is known as Mombacho's "main crater" is the space that was created by the slippage to the southeast. Volcanism at Mombacho seems to be younger in part than the Apoyo collapse and a young flow from Mombacho is composed of 18,000 ± 3,000 year old andesite. There are cinder cones and maars associated with fissure-type processes between Apoyo and Masaya calderas, as well as to the west and northwest of Mombacho volcano, contemporary with both centres.

Although the area's northeast, east and southeast margins lie at the same low elevations as Lake Nicaragua, most of the terrain is located at elevations of several hundred meters, in permeable rocks that constitute good aquifers. Water supply wells in the area's central zones are 100-300 m deep. Under the permeable strata, there are virtually impermeable rocks composed of sandstone and shale, to which only fracturing originating from deep tectonics has given some vertical permeability.

1.4 Surface manifestations

The area's geothermal manifestations include heavy fumarolic activity of volcanic origin in the Masaya complex, and fumaroles with temperatures of up to 99°C at the heights of Mombacho volcano's main crater. The Mombacho fumaroles have hydrothermal characteristics with some magmatic influence. To the south of the Mombacho fumaroles, but always within the main crater, there are several springs with a maximum temperature of 54°C. Further down, on the south plain, which is covered by clastic slide deposits, there is another group of thermal springs generally associated with swamps and lagoons, with temperatures that reach up to 60°C. Similarly, at the Mombacho volcano's northeast flank, among the slide deposits that exist in that direction, there is a thermal spring (38°C) at 200 m a.s.l. and another (55°C) at the level of Lake Nicaragua. To the south, hot springs at lower elevations result from shallow waters mixing with a deeper (and presumably hotter) Na-Cl (sodium-chloride) component. The Cl^- concentration in all these mixed fluids is very low.

Wells with minor thermal anomalies (31-34°C) are reported between the Apoyo caldera and the Mombacho volcano. There are no underground water sampling sites within the Masaya caldera. However, to the north there is a zone with wells at which temperatures reach a maximum of 38°C, which is probably due to the discharge in the north at the caldera bottom. Volcanism at Apoyo caldera provides a clear sign of prolonged magma residence at relatively shallow crustal levels and a vast magma chamber, which very probably generated a major subsoil thermal anomaly in the entire area surrounding the current Apoyo caldera (CNE, 2001).

1.5 Objective

The main goal of this project is to apply some common geochemical techniques to evaluate available chemical data for the Masaya-Granada-Nandaime geothermal area in Nicaragua.

2. LITERATURE REVIEW

2.1 Sampling techniques

The collection of samples for chemical analysis is the first step in a long process which eventually yields results that provide building blocks in the model of a geothermal system. This step has to be executed properly because all subsequent steps depend on it. The most common mistakes made during sampling involve the use of improper containers, improper cleaning and lack of or improper preservation of samples.

2.1.1 Sampling of hot springs and hot-water wells

When embarking on sampling of geothermal fluids from a particular field, it is very useful to have information on the distribution of the thermal manifestations in the area as well as on the temperatures and flow rates of the springs.

The intensity of surface activity between and within geothermal fields is highly variable. It may not be practical or serve a purpose to sample all springs in a particular field. Specific sites need to be selected for sampling. The criteria used to select hot springs for sampling include temperature, flow rate, geographic distribution, whether the water issues from soil or directly from the bedrock and any hydro-geological observations that might indicate mixing of the geothermal water with surface water. Generally speaking, the most favourable sites are springs with the highest temperature, the highest flow rate, the smallest aperture and minimum contact with any soil. Sampling and analysis of ground and surface waters is important for evaluation of possible mixing of the geothermal water with such shallow water in upflow zones (Arnórsson et al., 2006).

2.1.2 Sampling of fumaroles, dry-steam wells and gases from thermal springs

The selection of fumaroles for sampling is not as straightforward as that of hot springs. It is generally best to sample small outlets, which discharge steam at considerable velocity, in areas of the most intense acid surface alteration. Mud pools or pools of steam-heated surface water should be avoided, if possible. The gas phase discharged from such thermal manifestations tends to be low in H_2S compared to that of adjacent fumaroles because of its oxidation by oxygen dissolved in the surface water through which the steam passes (Arnórsson, 1987). Sampling fumarole steam provides information on individual gas concentrations in the steam and is, for this reason, also preferred to the sampling of gases bubbling through steam-heated or hot-spring water. The latter only provide information on the relative amounts of the gases in the gas phase and not their absolute concentrations in the steam. Warm, moist air emerging from hot ground may look like a fumarole. Temperature measurements will reveal that it is not. For this reason, it is useful to measure the temperature when collecting samples from fumaroles so as to eliminate any uncertainty about the nature of the discharge (Arnórsson et al., 2006).

2.2 Analysis of samples

Samples of geothermal waters can be preserved by appropriate treatment upon collection in such a way that later analysis in the laboratory provides reliable information on all component concentrations in the sample when collected. Several components can be conveniently analysed on site, including total carbonate carbon, sulphide sulphur and pH. At times, analysis on site may be necessary or preferred because of difficulties in preserving the samples with respect to these components. For example, water containing dissolved oxygen and some dissolved ferrous iron cannot be preserved for adequate pH measurement. Oxidation of the divalent iron and its subsequent precipitation as ferric hydroxide will lead to a decrease in the water pH. If samples are collected into airtight containers, however, pH and total carbonate carbon are best determined in the laboratory where the temperature is

stable. H_2S is most conveniently determined on site. Some parameters must always be measured on site, including temperature, flow rate and redox potential (Arnórsson et al., 2006).

2.3 Quality control of chemical analysis of geothermal water samples

The examination and interpretation of geochemical data can provide powerful tools for characterising geothermal systems and for monitoring the production of and injection into developed geothermal reservoirs. Chemical analyses have long been used to estimate subsurface temperatures, and computer simulations of multiple geochemical equilibria provide the means for predicting scaling and corrosion, for estimating loss of reservoir permeability from mineral precipitation, and for detecting breakthrough of injected water. Isotope analyses may provide qualitative indications of source areas and volumes for recharge to hydrothermal systems and are used to calculate additional estimates of reservoir temperatures. More complex geochemical calculations are not meaningful if the accuracy and precision of the analytical data used in such calculations are questionable.

It is common in studies of aqueous geochemistry to assume that chemical analytical concentrations are within 10% of the actual concentration of any constituent. For a reservoir temperature of 275°C, a 10% error in silica or sodium concentration will change the calculated temperature by about 10°C; and, for a reservoir temperature of 85°C, a 10% error in silica or sodium will change the temperature by 3-4°C (Reed and Mariner, 1991).

2.3.1 Evaluation criteria

The evaluation of a chemical analysis depends on the degree to which the analysis reflects the complete composition of the water sample. Many reports only include a partial analysis used for a specific purpose, and the quality of a partial analysis can rarely be evaluated. Chemical analyses can best be evaluated if they include the field measurement of pH, a complete suite of the major ions (Li, Na, K, Ca, Mg, F. Cl, SO_4, and HCO_3), and laboratory measurements of pH and conductivity. The chemical species of considerable geothermal interest (SiO_2, B, and Fe) should be added to the basic analyses. From the concentrations of the major ions, it is possible to calculate the charge balance and the conductivity balance for the sample.

Some general relationships are common for geothermal water samples. The concentrations of the cations usually follow a trend with Na > K > Li and Ca > Mg. Among samples from a single system, SiO_2 increases with increasing temperature. The occurrence of other major ions in the analysis, such as phosphate or nitrate, is normally an indication of contamination from surface water.

A few simple calculations can be used to determine the reliability of the chemical analyses. The ionic species are expressed as equivalent concentrations from the following calculation:

$$\text{Equivalent concentration} = \frac{\text{Concentration} \times \text{Ionic charge}}{\text{Molecular weight}} \quad (1)$$

where Molecular weight is in g/mole;
Concentration is in mg/l; and
Equivalent concentration is in meq/l.

Using equivalent concentrations of the ions, the error in charge balance is calculated from the absolute difference between the sums of cations and of anions divided by the average of the total cations and anions:

$$\text{Error (\%)} = \frac{\sum \text{cations} - \sum \text{anions}}{\sum \text{cations} + \sum \text{anions}} \times 200 \quad (2)$$

where Σcations is the sum of equivalent concentration of cations;
Σanions is the sum of equivalent concentration of anions.

The water can have no net electrical charge, so an error greater than 5% in the ionic charge balance is indicative of a problem and the analysis should be repeated. This limit is based on experience, and there must be a compromise between a restrictive limit that few samples would pass and a permissive limit that would ignore a significant error in a major ion.

If the electrical conductivity of a water sample is measured, a comparison can be made between the ionic charge and the electrical conductivity (referred to here as the conductivity balance). The calculation of error is based on an empirical relationship for the conductivity of sodium chloride solutions at 25°C. Different ions in solution act to increase or decrease the conductivity from that of sodium chloride, but the relation holds well for many natural waters (Hem, 1970). The error in conductivity balance was calculated using the following expression:

$$\text{Error (\%)} = \frac{\text{conductivity} - 100 \times \sum \text{cations}}{\text{conductivity}} \times 100 \quad (3)$$

where Conductivity is in standard units of (μS/cm); and
The sum of equivalent concentrations of cations (or anions) is first multiplied by 100.

The error in the electrical conductivity balance should be less than 10% for either anions or cations. Errors in charge balance of more than 5% or in conductivity balance of more than 10% and usually derived from three main sources: 1) an important ion was not analysed, 2) a mistake was made in an analysis of a major ion, and 3) a decimal point was misplaced. If the conductivity balance error is low for cations and high for anions, the anion analyses are the likely source of error. Calculations of error in charge balance and in conductivity balance only consider the ionic species. Some waters with high concentrations of unusual ions may repeatedly fail these tests (Reed and Mariner, 1991).

2.3.2 Correction of the carbonic species present in water samples taking into account the pH and temperature of the sample

The mass balance of carbonate species can be expressed as follows:

$$\left[CO_{2,T}\right] = [H_2CO_3] + [HCO_3^-] + \left[CO_3^{-2}\right] \quad (4)$$

where $[CO_{2,T}]$ is the total carbon carbonate content; if the alkalinity value was reported as bicarbonate content, that value has to be converted to the molar concentration, dividing the alkalinity value as bicarbonate ($Alc(HCO_3^{-1})$) with the molecular weight of bicarbonate (61.0061 g/mol).

The first dissociation reaction of carbonic acid is:

$$H_2CO_3 \leftrightarrow H^+ + HCO_3^- \quad (5)$$

The equilibrium constant K_1 for the last reaction is:

$$K_1 = \frac{\left[H^+\right] \times [HCO_3^-]}{[H_2CO_3]} \quad (6)$$

where $[H^+]$, $[HCO_3^-]$, $[H_2CO_3]$ correspond to the concentrations of each one expressed in ppm.

This constant, K_1, can be expressed as a temperature function as follows (Arnórsson et al., 1982):

$$\log K_1(T) = +6.38 - \frac{2107}{T} - 19.13\times10^{-3} \times T \tag{7}$$

where T is absolute temperature (K).

The second dissociation of bicarbonate is expressed by:

$$HCO_3^- \leftrightarrow H^+ + CO_3^{-2} \tag{8}$$

For the latter reaction, the equilibrium constant of the reaction can be calculated as follows:

$$K_2 = \frac{[H^+] \times [CO_3^{-2}]}{[HCO_3^-]} \tag{9}$$

This constant, K_2, can be expressed as temperature function as follows (Arnórsson et al., 1982):

$$\log K_2(T) = +4.40 - \frac{2589}{T} - 20.36 \times 10^{-3} \times T \tag{10}$$

where T is absolute temperature (K).

It can be assumed that the samples are highly diluted, so the activity coefficient of the species can be considered equal to one, therefore, the activity and concentration of species will have the same value. Multiplying Reactions 6 and 9 we get:

$$K_1 \times K_2 = \frac{[H^+] \times [HCO_3^-]}{[H_2CO_3]} \times \frac{[H^+] \times [CO_3^{-2}]}{[HCO_3^-]} = \frac{[H^+]^2 [CO_3^{-2}]}{[H_2CO_3]} \tag{11}$$

After the last operation, it is necessary to isolate $[CO_3^{-2}]$ as function of H_2CO_3 as follows:

$$[CO_3^{-2}] = \frac{K_1 \times K_2 \times [H_2CO_3]}{[H^+]^2} \tag{12}$$

From Reaction 6, it is necessary to isolate $[HCO_3^-]$ as a function of H_2CO_3 as follows:

$$[HCO_3^-] = \frac{K_1 \times [H_2CO_3]}{[H^+]} \tag{13}$$

Then substituting Reactions 12 and 13 into Reaction 4, we get the following expression:

$$[CO_{2,T}] = [H_2CO_3] + \frac{K_1 \times [H_2CO_3]}{[H^+]} + \frac{K_1 \times K_2 \times [H_2CO_3]}{[H^+]^2} \tag{14}$$

Now it is necessary to isolate the H_2CO_3 concentration as a function of total carbon carbonate content, dissociation constants of carbonic acid (K_1 and K_2) and the concentration of H^{+1} in solution. After some operations it is possible to get the following expression:

$$[H_2CO_3] = \frac{[CO_{2,T}]}{\left[1+\frac{K_1}{[H^+]}+\frac{K_1*K_2}{[H^+]^2}\right]} \quad (15)$$

Now it is necessary to substitute Reaction 15 into Reactions 12 and 13, which finally gives the following expressions:

$$[CO_3^{-2}] = \frac{K_1 \times K_2}{[H^+]^2} \times \frac{[CO_{2,T}]}{\left[1+\frac{K_1}{[H^+]}+\frac{K_1 * K_2}{[H^+]^2}\right]} \quad (16)$$

$$[HCO_3^-] = \frac{K_1}{[H^+]} \times \frac{[CO_{2,T}]}{\left[1+\frac{K_1}{[H^+]}+\frac{K_1 \times K_2}{[H^+]^2}\right]} \quad (17)$$

Equations 16 and 17 were used to calculate the expected concentrations of carbonate and bicarbonate species. These values were useful in finding the ionic balance for each sample. This method was used mainly to choose which records would be analysed using ternary diagrams (Giggenbach, 1991) and the speciation program Watch (Arnórsson and Bjarnason, 1993).

The $[H^+]$ content in solution has to be calculated using the next expression:

$$[H^+] = 10^{-pH} \quad (18)$$

The equations used to evaluate the ionic balance of each record were the following:

$$\text{sum of cations} = \left(1\times\frac{Na^+}{MW_{Na}}\right)+\left(2\times\frac{Ca^{+2}}{MW_{Ca}}\right)+\left(2\times\frac{Mg^{+2}}{MW_{Mg}}\right)+\left(1\times\frac{K^+}{MW_K}\right) \quad (19)$$

$$\text{sum of anions} = \left(1\times\frac{HCO_3^-}{MW_{HCO_3^-}}\right)+\left(2\times\frac{CO_3^{-2}}{MW_{CO_3^{-2}}}\right)+\left(1\times\frac{Cl^-}{MW_{Cl}}\right)+\left(2\times\frac{SO_4^{-2}}{MW_{SO_4^{-2}}}\right) \quad (20)$$

$$\%\text{ of difference} = 200 \times \left[\frac{\text{sum of cations - sum of anions}}{\text{sum of cations + sum of anions}}\right] \quad (21)$$

where MW is the molecular weight.

2.4 Interpretation methods

2.4.1 A diagnostic plot of water chemistry

Most geochemical techniques may, with confidence, be applied only to specified types of fluids with limited ranges of compositions. For instance, most ionic solute geothermometers work only if used with close to neutral waters containing chloride as the major anion. Any such interpretation of geothermal water samples, therefore, is best carried out on the basis of an initial classification, e.g. in terms of their major anions Cl, SO_4^{-2} and HCO_3^-. The simple Cl-SO_4-HCO_3 ternary plot can easily be constructed as follows:

1) Add the chloride, sulphate and bicarbonate concentrations:

$$[Cl^-] + [SO_4^{-2}] + [HCO_3^-] = \Sigma \quad (22)$$

2) Calculate the relative proportion of each component of this sum as a percentage:

$$\% Cl = \frac{[Cl^-]}{\Sigma} \times 100 \quad (23)$$

$$\%SO_4^{-2} = \frac{[SO_4^{-2}]}{\Sigma} \times 100 \quad (24)$$

$$\% HCO_3 = \frac{[HCO_3^-]}{\Sigma} \times 100 \quad (25)$$

The bicarbonate content represented by this diagram is the total concentration of all carbonate species in the water. This plot is very useful in identifying the various water types, and assists in recognising those waters which are most suitable for geothermometry (those closest to the Cl^- apex). Further, if data from the whole field area are plotted, then from the spatial position of spring and well discharges on the diagram, mixing trends and sub-surface flow directions can be identified. (Nicholson, 1993)

2.4.2 The Na-K-Mg diagram

Ionic solute geothermometers such as those based on Na-K (Ellis and Mahon, 1967), and Na-K-Ca contents (Fournier and Truesdell, 1973) provide powerful tools for the evaluation of deeper conditions within geothermal systems. Most of the problems in their use arise from their application to unsuitable samples. Initial weeding out on the basis of pH or their relative Cl^-, SO_4^{-2} and HCO_3^- contents, goes a long way towards improving their reliability. It is essentially based on the temperature dependence of the two reactions:

$$\text{K-feldspar} + Na^+ \leftrightarrow \text{Na-feldspar} + K^+ \quad (26)$$

$$2.8\ \text{K-feldspar} + 1.6\ \text{water} + K^+ \leftrightarrow 0.8\ \text{K-mica} + 0.2\ \text{chlorite} + 5.4\ \text{silica} + 2\ K^+ \quad (27)$$

They both involve the mineral of full equilibrium assemblage expected to form after isochemical recrystallization of an average rock under conditions of geothermal interest. Na, K and Mg contents of waters in equilibrium with this assemblage are accessible to rigorous evaluation. The theoretical temperature dependence of the corresponding concentration quotients may then be used to derive the two geothermometers:

$$T_{kn} = \frac{1390}{1.75 - \log \frac{[K^+]}{[Na^+]}} - 273 \quad (28)$$

and

$$T_{km} = \frac{4410}{14 - \log \frac{[K^+]^2}{[Mg^{+2}]}} - 273 \quad (29)$$

Again, it is based on the use of triangular diagrams. Because of the non-linear term $[K]^2$, the square root is taken of the Mg contents and the coordinates for the ternary diagram are calculated according to (Giggenbach, 1991):

$$S = \frac{[Na^+]}{1000} + \frac{[K^+]}{100} + \sqrt{[Mg^{+2}]} \quad (30)$$

$$\% \text{ Na} = \frac{[\text{Na}^+]}{10\text{S}} \tag{31}$$

$$\% \text{ Mg} = \frac{100\sqrt{\text{Mg}^{+2}}}{\text{S}} \tag{32}$$

where $[Na^+]$, $[K^+]$ and $[Mg^{+2}]$ = concentration of cation expressed as ppm.

2.4.3 Chloride waters

This water type, also known as "alkali-chloride" or "neutral-chloride", is typical of the deep geothermal fluid found in most high-temperature systems. The areas which contain hot, large-flow springs with the highest Cl^- concentration are fed more directly from the deep reservoir, and identify permeable zones within the field. However, these areas may not necessarily overlie the major upflow zone since the local topography can exert a significant control on the hydrology. Chloride fluid is commonly discharged from hot springs and pools of good flow, and from most geysers. The water in deep pools appears clear and blue-green in colour - a distinctive feature of chloride waters.

Chloride is the dominant anion, and usually attains concentrations in the thousands of mg/kg range, up to about 10,000 mg/kg. Other main constituents include sodium and potassium as the principal cations. The sodium-potassium ratio is dependent on temperature and this is the basis of the Na/K geothermometer. If the ratio is 10:1, the temperature is about 200°C, if the ratio is lower the temperature is higher and vice versa. Significant concentrations of silica are present (higher concentrations with increasing temperature at depth). Boron is extremely variable, possibly very high in sedimentary environments but quite low in some recent volcanic systems. Sulphate and bicarbonate concentrations are variable, but are commonly several orders of magnitude lower than that of chloride. The pH is invariably slightly acidic or alkaline, i.e. near-neutral, at the temperature of measurement. Carbon dioxide and much lower levels of hydrogen sulphide are the main dissolved gases. In fields with a high gas content, chloride fluids may contain high levels of bicarbonate and boil at greater depths. However, the high concentration of Cl^- prevents any confusion between these waters and the bicarbonate or diluted chloride-bicarbonate waters.

The discharge features are usually surrounded by silica sinter, which provides a guide to extinct hot springs, pools and geysers, and to subsurface temperatures in excess of 200°C. High-gas fields with significant bicarbonate concentrations can deposit an intimate mixture of sinter and travertine. These are the spring waters which can be used with most confidence in geothermometry. Hot chloride springs of good flow usually indicate a highly permeable feed zone (e.g. fault, eruption breccia pipe or conduit) (Nicholson, 1993).

2.4.4 Sulphate waters

These fluids are surface fluids often formed by the condensation of geothermal gases into near-surface, oxygenated groundwater, but sometimes, their origin can be related to equilibria deep down in geothermal systems and may even be useful for interpretation. The gases, with steam and other volatiles, were originally dissolved in the deep fluid but separated from the chloride waters following boiling at depth. They are found on the margins of a field some distance from a major upflow area, at topographic levels high above the water table, in perched water tables and over boiling zones. Although usually found near the surface at < 100 m depth, sulphate waters can penetrate to depth through faults into the geothermal system. Here they are heated, take part in rock alteration reactions and mix with the ascending chloride fluids (e.g. many fields in the Philippines). These acid waters are usually found in turbid (cloudy) pools or mud pools but may also occur as springs. As the separated steam contains a significant proportion of the enthalpy of the deep fluid, the steam-heated waters may boil at the water table to produce boiling mud pools and steaming ground. These hot, acidic waters can dissolve rocks to form large collapse craters and caves which often tend to plunge into the ground

at an oblique angle rather than vertically. Sulphate is the principal anion, and is formed by the oxidation of condensed hydrogen sulphide. The latter reaction and the condensation of carbon dioxide produce protons, creating acidic waters. The oxidation of hydrogen sulphide to sulphate ions produces a minimum pH of ~2.8. If waters are significantly more acidic than this (pH < 2), a magmatic gas contribution is likely.

Chloride occurs in trace amounts. Bicarbonate is either absent or at low concentrations since in very acidic waters the dissolved carbonate is usually lost from solution as carbon dioxide gas. Other volatile constituents which separate from the deep fluid on boiling may also condense into these waters (e.g. NH_3, As, B) and attain significant concentrations. Near-surface reactions between the acidic waters and the surrounding country rocks may leach silica and metal cations (Na, K, Mg, Ca, Al, Fe etc.) which can thereby attain high concentrations in the waters. No extensive deposits usually form around springs discharging sulphate waters, though native sulphur, alunite and other sulphates may be present. Since the concentration of silica and most cations is only the product of near-surface leaching, such steam-heated waters cannot be employed in geothermometry as the concentrations of the dissolved constituents bear no relation to mineral-fluid equilibria in the reservoir. As gases migrate more directly to the surface than waters, the spatial distribution of acid-sulphate features and acid-alteration may identify areas overlying a permeable boiling zone. However, some caution is required in such interpretation, since the presence of a horizon which is impermeable to both waters and gases will cause lateral flow of both phases; under such circumstances the presence of acid discharge features may only indicate a thinning of this migration barrier (Nicholson, 1993).

2.4.5 Bicarbonate waters

These waters, which include those termed CO_2-rich fluids and neutral bicarbonate-sulphate waters, are the product of steam and gas condensation into poorly-oxygenated sub-surface groundwaters. Such fluids can occur in an umbrella-shaped perched condensate zone overlying the geothermal system, and are common on the margins of fields. Bicarbonate waters found in non-volcanogenic, high-temperature systems (e.g. Turkey and Africa) are more problematic in origin and may constitute the deep reservoir fluid. The waters are of near-neutral pH as reaction with the local rocks (either in the shallow reservoir or during lateral flow) neutralises the initial acidity of these waters. Loss of protons in such reactions produces near-neutral waters with bicarbonate and sodium as the principal constituents. Sulphate may be present in variable amounts, with chloride at low concentrations or absent (Mahon et al., 1980). These waters are highly reactive, and their corrosive action on well casings needs to be taken into account in the development of a field.

Extensive deposits of travertine ($CaCO_3$) can form around bicarbonate springs, and can be indicative of subsurface temperatures of below 150°C. Aragonite can form if the surface discharge and cooling is very rapid.

Although such fluids may discharge from equilibrated shallow and deep aquifers within high-temperature systems, there exists doubt about their use in geothermometry. Most geothermometer equations have been derived from data on chloride fluid equilibria and their application to a different fluid type is questionable. Application of the Na-K-Ca geothermometer to Na-HCO_3 fluids has been described as "troublesome" (Fournier, 1989). Certainly, where these waters are formed by steam-heating/condensation, their chemistry is unrelated to equilibria in the deep reservoir fluid, making geothermometry inappropriate (Nicholson, 1993).

2.4.6 Sulphate-chloride

These waters can be formed by several processes, and the following have been suggested:

a) Mixing of chloride and sulphate waters at variable depths;
b) Near surface discharge and oxidation of H_2S in chloride waters;

c) Near-surface condensation of volcanic gases into meteoric waters;
d) Condensation of magmatic vapour at depth;
e) Passage of chloride fluids through sulphate-bearing sequences (e.g. evaporites) or lithologies containing native sulphur.

The waters formed by process (a) are probably the most usual, and it is these which are discussed below unless otherwise stated. These waters are typically of pH 2-5, with chloride and sulphate in approximately equal proportions. Waters formed by processes (c) and (d) can be recognised by the very high concentrations of Cl^-, SO_4^{-2} and, most diagnostic, high F. These waters may also be unusually acidic with pH 0-2; however, rock-water neutralisation reactions can raise the pH and mask this characteristic feature. Waters that have passed through native sulphur at depth (process e) may remobilise the mineral and deposit distinctive yellow sulphur around the spring.

It is often stated that as these fluids are a mixture containing the deep chloride fluid, geothermometry can therefore be applied with confidence. This is an erroneous argument since the composition of the mixed water will probably contain silica, sodium, potassium and other cations contributed by the acid component, and this will distort the results of solute geothermometry. Any application of geothermometers to mixed fluids must therefore be interpreted with caution (Nicholson, 1993).

2.4.7 Dilute-chloride (bicarbonate) waters

These waters are formed by the dilution of chloride fluid by either groundwater or bicarbonate water during lateral flow. They are probably restricted to the margins of major upflow zones and outflow structures of high-temperature systems. They are often discharged from springs in low-temperature systems. They can be near-neutral waters, typically, pH is 6-8 with chloride as the major anion and with bicarbonate present but in variable concentrations.

If the chloride waters have been diluted by groundwater only, then geothermometry may be applicable. However, some discretion is needed since dilution will affect the silica geothermometer and the addition of bicarbonate may cause problems with the Na-K-Ca technique. In addition, during lateral flow, Li can be lost by adsorption and Mg can be added by near-surface reactions, throwing into question the reliability of the Na/Li and K/Mg methods. Even if the application of geothermometers is suspect, the spatial distribution of these springs is important in understanding the hydrology of the system. In this respect it is important to recognise waters of this type as "dilute-chloride" and not refer to them as "bicarbonate" waters which are genetically very different. This point is made because the term "bicarbonate water" is often used in some reports in a casual manner to mean any spring waters containing significant bicarbonate, but not necessarily steam-heated in origin (Nicholson, 1993).

2.5 Geothermometry

Chemical and isotope geothermometers probably constitute the most important geochemical tools for the exploration and development of geothermal resources. They are also very important during production in monitoring the response of geothermal reservoirs to the production load. During the exploration phase, geothermometry is used to estimate subsurface temperatures, i.e. temperatures expected to be encountered by drilling, using the chemical and isotopic composition of hot spring and fumarole discharges. During the later phases in geothermal development and monitoring, geothermometry has been successfully applied to interpret the composition of well discharges with respect to locating the levels of producing horizons in the wells. Geothermometry is also useful in elucidating chemical reactions occurring in the zone of depressurisation around wells that result from boiling and/or cooling by recharging cold water.

Geothermometers have been classified into three groups:

1) Water or solute geothermometers;
2) Steam or gas geothermometers;
3) Isotope geothermometers.

When geothermometers are applied to estimate subsurface or aquifer temperatures, a basic assumption is always made, namely that temperature dependent chemical or isotopic equilibria prevail in the source aquifer. Further, as stated above, the approximation is made that chemical and isotopic reactions do not significantly modify the composition of the fluid as it ascends from the source aquifer to the point of sampling, whether it be a thermal spring, a fumarole or a wellhead.

Experience shows that results for different chemical and isotope geothermometers sometimes compare well for a particular discharge although sometimes large differences are seen. Good conformity between individual geothermometers is usually taken to indicate that the assumption of equilibrium is valid and that faith can be put into the results. Discrepancy in results, on the other hand, is indicative of disequilibrium. A discrepancy may, however, be utilised to quantify various processes in geothermal systems such as boiling and mixing with cooler water in upflow zones. Therefore, differences in the results of individual geothermometers need not be a negative outcome for their interpretation (Arnórsson, 2000).

2.5.1 Quartz geothermometers

The silica content of water samples can be used to predict the subsurface temperature of aquifers or reservoirs by applying silica geothermometers. A limiting temperature for silica geothermometry tends to be about 250ºC, since above this temperature silica dissolves and precipitates very rapidly, too rapidly for the silica concentration in solution to remain constant as the fluids are discharged to the surface (Nicholson, 1993).

As the geothermometer is dependent on an absolute concentration, rather than a ratio of concentrations, it is affected by physical processes such as boiling and dilution. These processes need to be recognised and, where possible, corrections should be made through the use of alternative geothermometry equations or the silica mixing model. Note also that silica can be added by mixing with acidic near-surface fluids. Under such circumstances, the silica content of the discharged mixed water will not be representative of the reservoir concentration, and geothermometer temperatures will be misleading. The deduction of geothermometer equations for quartz is based on the solubility reaction of quartz as follows:

$$SiO_2 + 2H_2O = H_4SiO_4^o \tag{33}$$

The equilibrium constant for this reaction is given by:

$$K_{eq} = \frac{[H_4SiO_4]}{[SiO_2][H_2O]^2} \tag{34}$$

where brackets indicate the activity of the respective species and phases.
The activity of pure phases is equal to 1. In general, quartz does not contain impurities to any significant extent and, if the water is dilute, its activity is close to 1, in which case Equation 34 reduces to:

$$K_{eq} = [H_4SiO_4] \tag{35}$$

Consequently, after applying an expression of the van´t Hoff equation to Equation 36, it is possible to obtain the following expression:

$$\mathrm{Log}(K_{eq}) = \frac{1}{T} \times \frac{-\Delta H^o}{R \times 2.303} \tag{36}$$

where K_{eq} is the equilibrium constant;
T the temperature in K;
ΔH^o, the enthalpy of the reaction in kJ/kg; and
R is the gas constant.

For many silicate-water reactions, it is a good approximation, at least up to about 250°C, to take the enthalpy of such reactions to be constant. This expression is particularly useful when experimental or drillhole data, which are used to calibrate geothermometers, only cover a limited temperature range and need to be extrapolated, either to lower or higher temperatures.

2.5.2 Chalcedony geothermometer

There is an ambiguity in the use of silica geothermometers at temperatures less than about 180°C because chalcedony appears to control dissolved silica in some places and quartz in others. Chalcedony is a very fine grained variety of quartz composed of aggregates of very tiny crystals. The individual quartz grains are so small that they have relatively large surface energies compared to "normal" quartz, and this results in an increase in solubility. Chalcedony is unstable in contact with water at temperatures above about 120-180°C because the smallest sized crystals dissolve completely relatively quickly and larger sized crystals grow large enough so that surface energy is no longer a factor. Temperature, time, fluid composition, and prior history (recrystallization of amorphous silica versus direct precipitation of quartz), all affect the size attained by quartz crystals. Thus, in some places where water has been in contact with rock at a given temperature for a relatively long time (many hundreds to thousands of years), such as in some deep sedimentary basins, quartz may control dissolved silica at temperatures less than 100°C. In other places, chalcedony may control dissolved silica at temperatures as high as 180°C (particularly newly fractured portions of hydrothermal systems). The mathematical deduction of this geothermometer is exactly the same as that presented in Section 2.5.1.

2.5.3 Cation geothermometers

Na/K ratios in geothermal waters were initially used to locate the major upflow zone in the Wairakei geothermal field in New Zealand (Ellis and Wilson, 1960), the lowest ratios being closest to the major upflow. Already at this time, the opinion was expressed that the Na/K ratios of geothermal waters were probably controlled by the equilibrium between the geothermal water and alkali feldspars. Many geochemical (empirical) calibrations have been proposed for the Na/K geothermometer. They reflect two things: many researchers have observed that Na/K ratios of geothermal waters relate to water temperature and that thermodynamic data have not been sufficiently accurate for theoretical calibration, or minerals other than feldspars are involved in the control of aqueous Na/K ratios.

Reactions between alkali feldspars and Na and K in aqueous solution have often been described as exchange reactions. At the temperature prevailing in geothermal systems (upto 350°C), this is probably not true, at least in the sense that Na and K do not exchange for each other and equilibrate with a mixed alkali feldspar. The reaction in question involves simultaneous equilibrium between Na^+ and K^+ in solution and quite pure albite and K feldspar. The reaction involved is appropriately expressed as:

$$NaAlSi_3O_8+K^+ \rightarrow KAlSi_3O_8+Na^+ \quad (37)$$

As the respective feldspars are almost pure, i.e. their activity is 1 (Arnórsson, 2000), hence the equilibrium constant, K_{eq}, for this reaction is:

$$K_{eq} = \frac{[Na^+]}{[K^+]} \quad (38)$$

where $[Na^+]$ and $[K^+]$ are the concentration of the respective ions expressed in molalities.

Concentration of the dissolved constituents can also be expressed in other units, such as mili-equivalents, ppm, or mg/kg, with the value of K_{eq} adjusted accordingly.

For an exchange reaction involving monovalent and divalent ions, such as K^+ and Mg^{+2}, the equilibrium constant (K_{eq}) is approximately equal to:

$$K_{eq} = \frac{[K^+]}{\sqrt{[Mg^{+2}]}} \tag{39}$$

where $[K^+]$ and $[Mg^{+2}]$ = concentration of the respective ions expressed in molalities.

The last part of the mathematical deduction of the geothermometer equation is the same as presented in Section 2.5.1.

2.5.4 Gas geothermometers

In many geothermal fields, surface manifestations consist only of hot ground, acid surface waters and fumaroles. In these fields the thermal groundwater table is subsurface. When this is the case, water geothermometers cannot be applied. This has called for the development of steam (gas) geothermometers for geothermal exploration. The first gas geothermometers were developed by Tonani (1980) and D'Amore and Panichi (1980). Later geochemical methods involving gas chemistry were developed to estimate steam to water ratios in geothermal reservoirs (e.g. D'Amore and Truesdell, 1985; Arnórsson et al., 1990).

There are essentially three types of steam geothermometers, those based on:

1) Gas-gas equilibria;
2) Mineral-gas equilibria involving H_2S, H_2 and CH_4 but assuming CO_2, to be externally fixed according to empirical methods;
3) Mineral-gas equilibria.

The first two groups of geothermometers require only data on the relative abundance of gaseous components in a gas phase, whereas the third group calls for information on gas concentrations in steam.

In three respects, steam geothermometry is more difficult to handle than water geothermometry. Firstly, gas concentrations in geothermal reservoir fluids are affected by the ratio of steam to water of that fluid. Secondly, the gas content of fumarole steam is affected by the boiling mechanism in the upflow, steam condensation and the separation pressure of the steam from parent water. Thirdly, the flux of gaseous components into geothermal systems from their magmatic heat source may be quite significant and influence how closely gas-gas and mineral-gas equilibria are approached in specific aquifers. The components of water geothermometers are, on the other hand, with few exceptions solely derived from the enclosing rocks. Only if the recharging fluid is saline, as is the case with sea water, some aqueous components of water geothermometers are externally derived (Arnórsson, 2000). A list of the geothermometers applied in this study is found in Table 4 in Appendix I.

2.6 Isotopes

Isotope analysis of water samples from springs and wells gives information on the origin of the fluid discharged, on their age, on possible underground mixing between different waters, on water-rock

interaction, and on steam separation processes. Studies of the stable isotopes of geothermal gases may offer particular advantages with respect to studies of aqueous fluids, as the gases and their stable isotopes will be less affected by near surface conditions. We can therefore reach relatively reliable conclusions on the origin and evolution of the geothermal fluids. The isotopic compositions of the gases, carbon dioxide, methane and hydrogen are then evaluated for information on their origin and their usefulness for isotope geothermometry (Nuti, 1991).

Extensive use of fractions or ratios is made in isotope chemistry and this requires the introduction of some new terms. They are useful to avoid using lengthy expressions. The isotopic mass ratio in the sample, R_x, is always written with the heaviest isotope as the numerator (e.g. $^{18}O/^{16}O$ and D/H). The need for this notation arises from the way in which isotopes are measured by a mass spectrometer. This instrument determines the ratios of abundance of the different isotopes in a sample, not the concentration. However, it is difficult to determine the absolute ratio accurately and not practical to do so when analysing large numbers of samples on a routine basis. To overcome this, the isotopic ratio in the sample is compared to that in a well-defined standard which is simultaneously analysed. This gives rise to the expression:

$$\frac{R_x - R_{std}}{R_{std}} \tag{40}$$

where R_x is the isotopic mass ratio of sample; and
R_{std} is the isotopic mass ratio of the standard (SMOW).

The units of measurement for these isotopic ratios are parts per thousand (ppt) usually called *per mille* (‰) and given the notation delta (or "del"):

$$\delta_x\ (‰) = \left[\left(\frac{R_x}{R_{std}}\right) - 1\right] \times 1000 \quad \text{or} \quad 10^3 + \delta_x\ (‰) = 10^3 \times \left(\frac{R_x}{R_{std}}\right) \tag{41}$$

Prior to the development of isotope analytical techniques, it was uncertain whether geothermal waters had a magmatic or meteoric origin. However, Craig (Craig et al., 1956; Craig, 1963) demonstrated that the δD (Deuterium) content of geothermal waters is similar to that of local meteoric water, while the $\delta^{18}O$ (Oxygen 18) value of the geothermal water is sometimes more positive than that of meteoric water. Such an isotopic signature indicated that any magmatic contribution must be small (5 - 10% of the total fluid, otherwise the δD values of geothermal and meteoric water would not be similar) and that the bulk of the geothermal fluid must be of meteoric origin. This model of geothermal systems recharged by local meteoric water was further supported by the leaching experiments of Ellis and Mahon (1964) (Nicholson, 1993).

Since, at low temperatures, both ^{18}O and D fractionate into the condensed phase, water vapour in the atmosphere becomes increasingly depleted in these heavier isotopes upon precipitation and progressive movement towards the poles, to greater altitudes and inland, away from the ocean. The $\delta^{18}O$ value of meteoric waters at any locality is therefore dependent upon latitude, altitude and distance from the ocean. This variation is systematic, and Craig (1961) showed that on a global scale the hydrogen-oxygen isotope signature for fresh-waters could be defined by

$$\delta D = 8\ \delta^{18}O + 10 \tag{42}$$

where δD is the Deuterium content in ‰; and
$\delta^{18}O$ is the Oxygen 18 content in ‰.

The line defined by this equation is termed the *meteoric water line*. Local variations of this relationship do exist, although the slope is usually constant at around 8.

Reaction with the host rocks at depth alters the original isotopic signature of the meteoric water to that characteristic of geothermal waters. However, this can be then further changed by several sub-surface processes as the geothermal water rises to the surface. Some processes can shift the isotopic composition of the fluid. Of those it is possible to include: Rock water reactions, boiling, conduction, mixing and steam heating/surface evaporation (Nicholson, 1993).

2.7 Mixing processes

The use of chemical and isotope geothermometers to estimate subsurface temperatures from the composition of surface discharges is based on the notion that geothermal fluids may cool in upflow zones, either conductively or by boiling due to depressurisation, or by both processes. However, hot waters ascending from a geothermal reservoir may also cool by mixing in the upflow with shallow, relatively cold water. When this is the case, geothermometers applied directly to analytical results may yield misleading results.

Mixing of geothermal water with cold water may occur after a variable amount of conductive cooling of the hot water before, during or after boiling. Mixing is most prone to occur where there is a change in permeability. Drillings have shown that the pressure potential in the upflow of many geothermal systems is lower than in the enveloping cold groundwater body. When this is the case, cold groundwater tends to enter the geothermal system and mix with the rising hot water. At the boundaries of geothermal systems where hot and cold waters meet, local mixing brings about mineral deposition that reduces permeability and seals off the hot and cold groundwater systems. This seal impedes the incursion of cold water into the geothermal system, thus reducing the likelihood of mixing. Since concentration of dissolved solids is most often lower in cold waters than in geothermal waters, mixing is often referred to as dilution. Large variations in the temperature and flow rates of thermal springs in a particular field that can be linked with parallel variations in the concentrations of non-reactive components in the water, such as Cl^-, usually constitute the best evidence that mixing has occurred (Arnórsson, 2000).

It is necessary to establish that the waters sampled and analysed are truly mixed before applying mixing models to estimate reservoir temperatures. Assuming mixing for unmixed waters and applying mixing models can yield erroneous results which are generally too high. Linear relationships between the concentrations of conservative components, such as between Cl^- and B or Cl^- and δD, are generally considered to constitute the best evidence for mixing. A linear relationship between CI and $\delta^{18}O$ has also proved to be useful in cases where hot waters show a significant oxygen shift. A near linear relationship between chloride and silica has been observed for variably mixed waters in some geothermal fields. Such a relationship implies that silica behaves as a conservative component after mixing. In other words, the mixed water neither precipitates silica nor dissolves it from the rock to any extent. Such behaviour for silica is indeed assumed when using the silica-enthalpy warm spring and the silica-carbonate mixing models. Conservative behaviour of silica is also assumed when quartz equilibrium temperatures are used to create a chloride-enthalpy mixing model (Arnórsson, 2000).

Mixing of two waters can be indicated in a plot of one conservative species against another (conservative chemical species are comparatively inert and do not precipitate or react with rock minerals). The plot generally shows a well-defined mixing line that extends from the composition of one end member to that of the other. The pure end members may not have been sampled and do not necessarily appear on the plot. Points off the mixing line may indicate analytical error or a third fluid component. Constituents that may be conservative in one temperature range may be reactive in another. For example, silica, which reacts slowly at low temperatures and shows mixing reactions with chloride, may precipitate at higher temperatures (above ~ 200°C) and fall below the line. Stable isotope concentrations in water are generally conservative: deuterium, because there is negligible hydrogen in rocks; and oxygen-18 because an exchange with oxygen in rock minerals takes place mainly in high-temperature reservoirs. Enthalpy is also conservative in the absence of boiling and can

be used in a mixing plot. If the cold end member is very dilute, then the ion ratios of the more saline thermal water will be preserved in the mixed waters. This is also the case for mixing with more concentrated cold waters. If they are low in specific geothermal components such as Li, F or B. even Cl^- may fall in this group if the mixing cold water is $NaHCO_3^-$, SO_4^{-2} type, as is often the case (Truesdell, 1991).

Another method of showing mixing for a larger number of constituents is a Schoeller diagram. This diagram compares the log concentrations of fluid constituents from a number of analyses, with constituents of each analysis connected with a line (symbols and line patterns may be used to identify analyses). Because logarithmic values are used a wide range of concentrations can be shown. The effect of mixing with dilute water (as well as gain or loss of steam) is to move an analysis vertically without changing its shape. Slopes of lines between constituents represent concentration ratios. These diagrams show the effect of mixing on a number of constituents. When many analyses are represented, individual patterns may be lost, but the pattern of mixing will remain clear. The thermal waters have higher concentrations of Li, Na, K, F, Cl, SO_4 and B; the cold waters have higher Mg and Ca and almost the same HCO_3^- as the thermal waters. This diagram is more effective than a table in showing this mixing and serves as an introduction to the area's water chemistry (Truesdell, 1991).

2.8 Speciation using WATCH

Using the activities of aqueous component species calculated for homogeneous equilibrium at a series of temperatures, it is possible to compute the degree of super or under saturation of the aqueous phase with minerals at each temperature. This is expressed for mineral k in terms of log $(Q/K)_k$:

$$\mathrm{Log}\left(\frac{Q}{K}\right)_k = \log \prod a_{i,k}^{vi,k} - \log K_k \qquad (43)$$

where Q is the activity product for mineral k;
K is the equilibrium constant for mineral k;
$a_{i,k}$ is the activity; and
$v_{i,k}$ is the stoichiometric coefficient of component species i in the equilibrium mass action expression for mineral k, written with the mineral on the left hand side.

The numerical value of log $(Q/K)_k$ is greater than zero for supersaturated minerals and less than zero for undersaturated minerals. Since mineral mass action expressions are written only in terms of the component species listed above, the stoichiometry of all such expressions used here to compute log(Q/K) can be deduced from knowing the mineral formula and the set of component species.

The study of log(Q/K) diagrams for many geothermal and hot spring waters has shown that most waters closely approach equilibrium with a subsurface mineral assemblage, and that the calculated mineral equilibration temperatures are within 10-20°C of the measured temperatures or those determined from conventional chemical geothermometry. In cases where the Na-K-Ca and related methods fail to yield correct temperatures, the mineral equilibration method often still yields good temperature estimates because it is independent of assumptions of any particular mineral equilibria. It has been found that the Q/K plots have worked well for low-temperature springs as well as high temperature geothermal waters, both of widely variable composition (Reed and Spycher, 1984).

To carry out the previously mentioned calculation the computer program WATCH was used. This program is mainly intended to serve as a tool for interpreting the chemical composition of geothermal fluids, although it is also useful for non-thermal waters. The program uses the chemical analysis of water, gas, and steam condensate samples, collected at the surface, and computes the chemical composition of down-hole or aquifer, fluids. This includes the pH, aqueous speciation, partial pressures of gases, redox potentials, and activity products for mineral dissolution reactions.

3. INTERPRETATION OF RESULTS

The area under study comprises a region of about 1100 km^2 and the locations of the water samples collected during reconnaissance studies are not evenly distributed over the region but clustered around specific sites (Figure 2). The area was divided into the seven following regions: Masaya, Granada city, Apoyo lagoon, Mombacho north side, Mombacho volcano, Mombacho south side and Nandaime.

The first step of the data interpretation was to select the best set of records among the total initial data. This task was carried out by applying the criteria of Section 2.3. Also rejected were records that lacked geographical coordinates, temperature sampling, pH samples, and concentrations of two or more main ions. The summary of the data analysed is presented in Tables 1-3 in Appendix I.

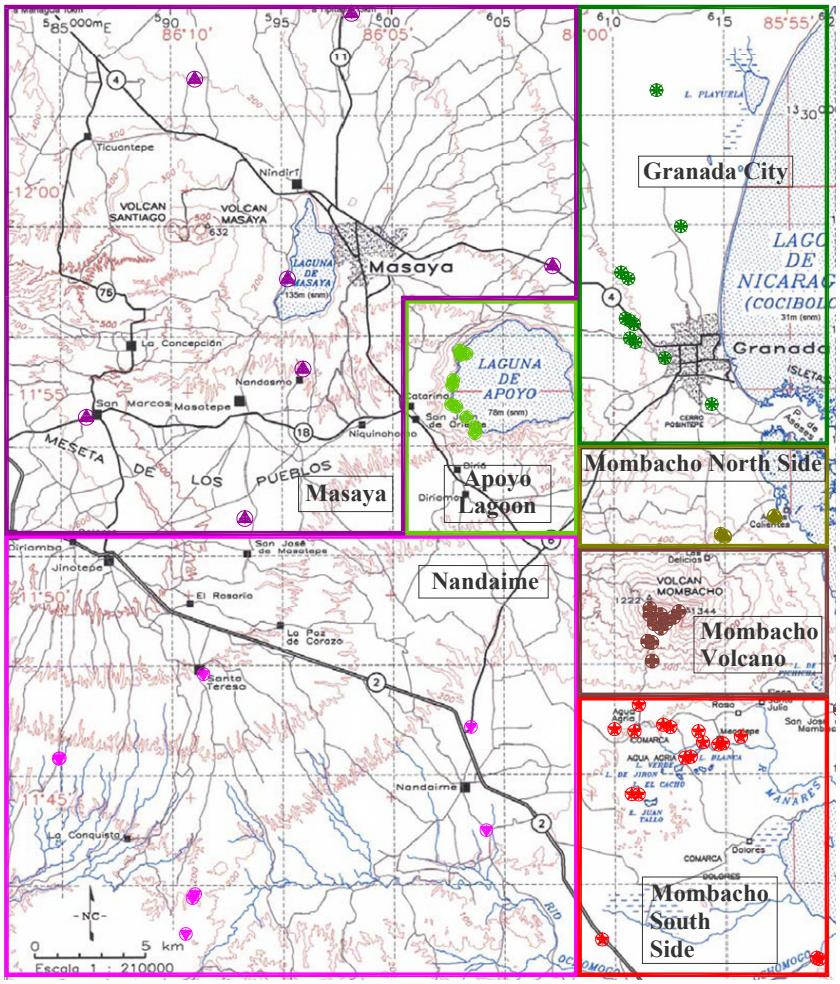

FIGURE 2: Division of the Masaya-Granada-Nandaime area and location of sampling points

3.1 **Ternary plot** (Giggenbach, 1991)

The analytical results for the water samples from each region were plotted individually and the trend that was observed in each region made it possible to combine and analyse them in the same graph. The application of the anion ternary graph presented in Figure 3 made it possible to identify, at least theoretically, the potential existence of a geothermal system, if we take into account the following facts:

The Apoyo Lagoon and Granada City samples exhibit the highest chloride content of all the samples, sodium being the major cation, followed by calcium and potassium, respectively. The pH values ranged from 6.67 to 8.4 and the highest temperature in the whole region 96.5°C was observed in Apoyo Lagoon area. The temperatures of the Granada City manifestations are low, with 28.4°C as the average temperature. These samples could be considered chloride waters but there are some departures from deep geothermal fluid behaviour: the silica content does not increase with temperature, and the magnesium content is extremely high compared with that of deep geothermal fluids. These observations suggest that the waters may be mixed.

Mombacho volcano samples plot mainly in the region of sulphate and steam heated waters. The average pH of these waters is 7.65, which is unusual for this kind of water, as it has been claimed that steam heated waters are usually acidic if we consider the addition of protons during the oxidation of

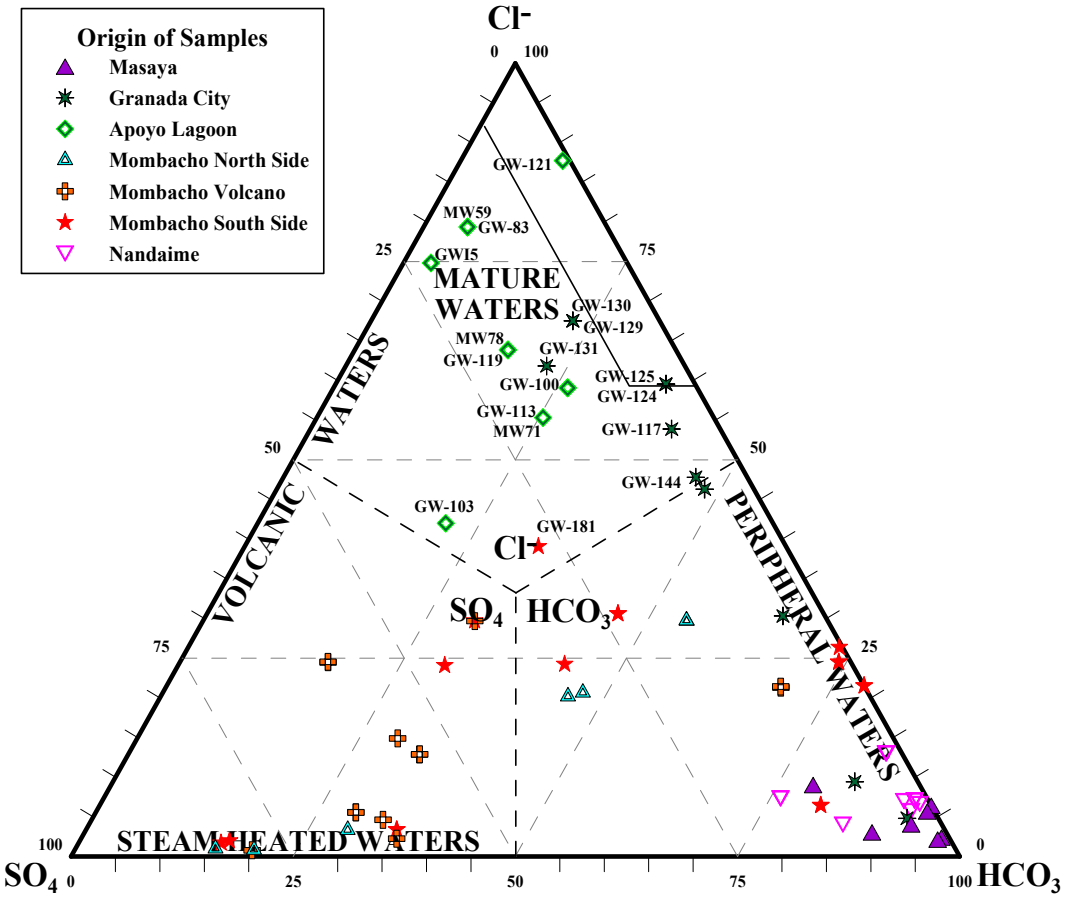

FIGURE 3: HCO_3-Cl-SO_4 ternary plot for the Masaya-Granada-Nandaime water samples

hydrogen sulphide and condensation of carbon dioxide (Nicholson, 1993). The water temperatures range from 26 to 49°C.

The samples from Mombacho north side and Mombacho south side are partially composed of bicarbonate waters and steam heated waters; only sample GW-181, which barely plots in the chloride region, can be considered showing different kind of waters. The temperatures of the north side samples (ranging from 36 to 54°C) are higher than the south side ones which range from 24 to 45°C; the average pH value of water from both regions is near-neutral. These waters are interesting for the high silica content of some samples: on the north side GW-56, GW-54, GW-I3, GW-42 and on the south side GW-181, GW-198. These peak values also coincide with the higher temperature values found in both regions.

The Masaya and Nandaime samples were bicarbonate waters, with few exceptions. All of them are located in the bicarbonate apex; the TDS values found in these samples are the lowest for all the geothermal areas. The temperature shows the same trend, so these waters could be considered typical surface waters.

Based on the investigation of all the regions comprising the Masaya-Granada-Nandaime geothermal area it is possible to suggest that the Apoyo Lagoon is the most permeable zone and could also be the main core of a geothermal system. We consider the waters of Mombacho Volcano, Mombacho North Side and Mombacho South Side to be mainly composed of steam heated waters that may be located on the margins of a geothermal field, some distance from a major upflow zone (Nicholson, 1993).

According to Figure 3, only samples GW-124, GW-125 and GW-121 are suitable for geothermometer application.

3.2 Na-K-Mg Ternary graph (Giggenbach, 1988)

The results for the Masaya Granada Nandaime water samples were plotted on a Na-K-Mg diagram shown in Figure 4. As can be seen, most of the samples plot in the magnesium corner and in the immature waters zone, which can be explained by mixing with shallow waters.

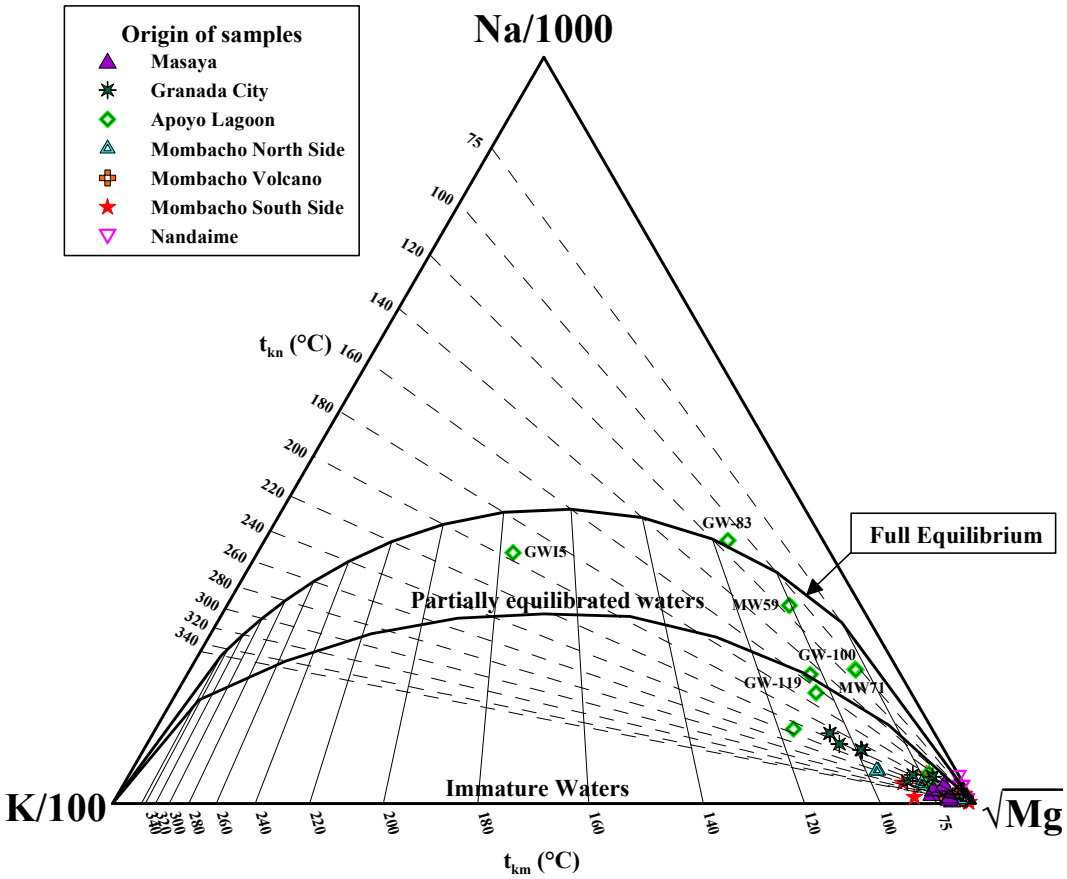

FIGURE 4: Na-K-Mg ternary plot for the Masaya-Granada-Nandaime water samples

Only sample GW-83 plots on the full equilibrium curve, according to the theory related to this technique, indicating that cation geothermometry can be applied with confidence to GW-83. Three of the other samples plot close to the full equilibrium curve and are probably in equilibrium, whereas two plot virtually on the partial equilibrium border curve and are probably mixed; the remaining samples appear to be predominantly composed of immature water.

In many cases the water has probably dissolved constituents from surface layers and is not suitable for interpretation with respect to deep water chemistry.

3.3 Geothermometry

3.3.1 Silica geothermometer

The silica geothermometers were only applied to water samples located in the chloride zone according to Figure 3; the geothermometer equations, the codes used to identify the different geothermometers are presented in Tables 4 in Appendix I and the temperatures predicted in Table 5. The geothermometry predictions for Granada City and Apoyo Lagoon water samples are shown in Figures 5 and 6, respectively.

Granada City

The estimated average temperature for this region is 83.9°C. Note that most of the samples are clustered in a band ranging from 56.2 to 103.4°C. Samples GW-131 and GW-144 showed very different profiles: GW-131 gave by far the highest temperature prediction in this region ranging from 116.1 to 144.3°C and can possibly be considered a mix of deep hot water with shallow water; on the other hand, GW-144 showed the lowest temperature prediction in this region ranging from 20 to 60°C. The temperatures predicted by quartz geothermometers 5 and 6 are lower than those predicted by 1, 2, 3 and 4. These differences gradually became smaller as the silica content in the water increased. The temperatures predicted by the chalcedony geothermometer were the lowest, as was expected.

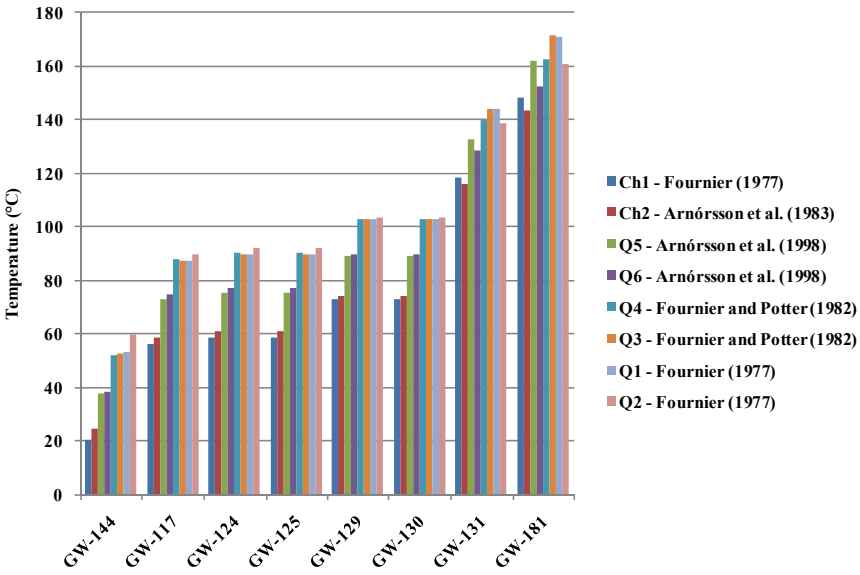

FIGURE 5: Quartz and chalcedony temperatures, predicted for Granada City water samples and GW-188 from Mombacho South Side

Apoyo Lagoon

The temperature predictions in Apoyo Lagoon region indicate the possible presence of hot fluids, as can be seen for samples MW78, GW-119, GW-113 GW-103 and GWI5; the average temperature from these predictions was 135.3 ºC, and the highest temperature 161.6 ºC, predicted for sample GWI5.

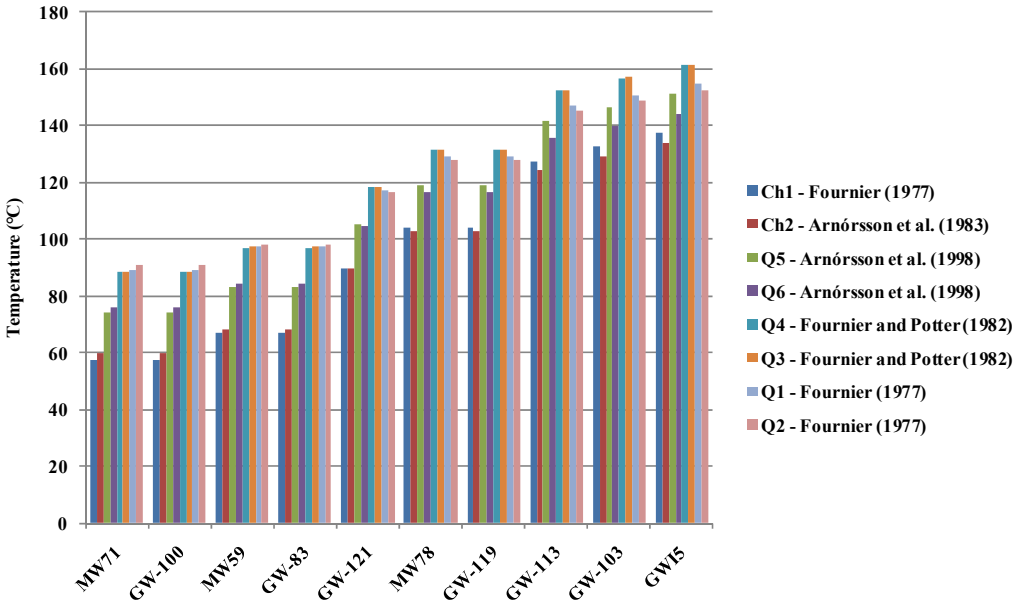

FIGURE 6: Quartz and chalcedony temperatures, predicted for Apoyo Lagoon water samples

3.3.2 Cation geothermometry

The temperatures predicted by applying these geothermometers for Granada city and Apoyo Lagoon water samples are shown in Figures 7 and 8, respectively. The equation codes used to identify every geother-mometer equation and actual results are given in Tables 4 and 6 in Appendix I. The predictions were arranged to perceive a stepwise pattern. The Na/K geothermometers were identified with the code "Na" and "a number", the K/Mg geothermometer was identified with the code "K1" and Na-K-Ca geothermometer was marked Na-K-Ca.

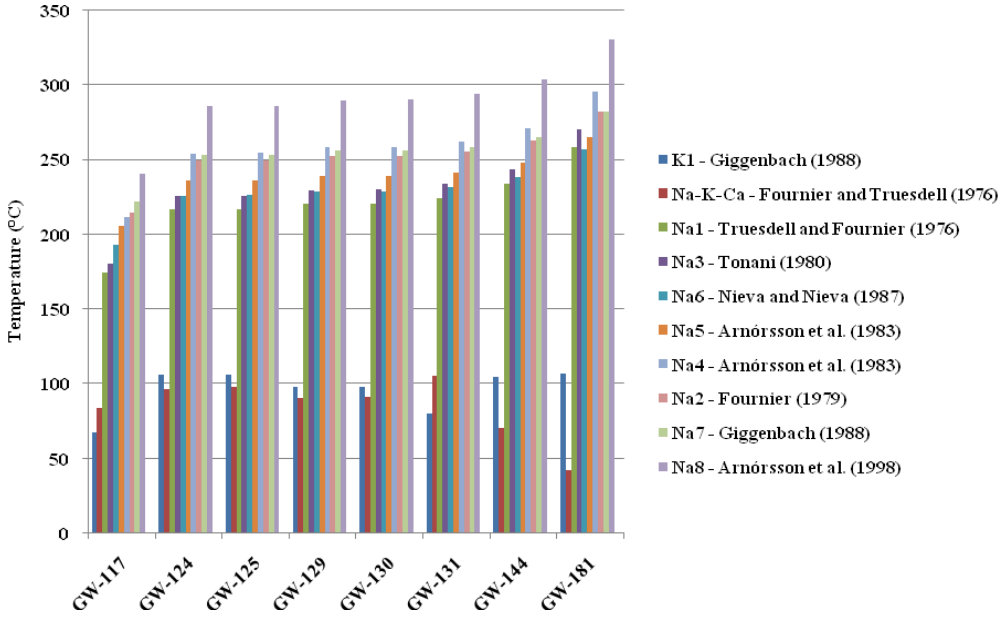

FIGURE 7: Cation ratio temperatures, predicted for Granada City water samples, and GW-181 from the Mombacho South Side

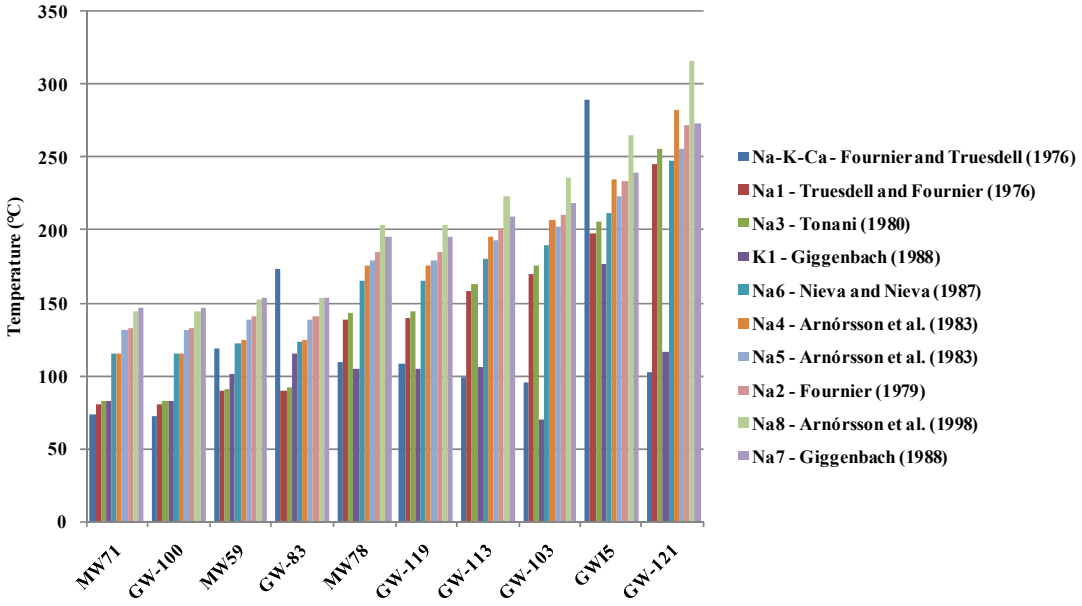

FIGURE 8: Cation ratio temperatures, predicted for Apoyo Lagoon water samples

Granada City

The temperatures predicted by K/Mg were, as usual, the lowest for every sample. This behaviour can be explained considering the results obtained in Figure 4. As can be seen, none of the Granada city samples plotted on the full equilibrium curve; instead they were clustered around the Mg apex in the immature water zone. This conduct is usual for water with high magnesium content, probably

contributed by shallow waters. The K/Mg geothermometer equilibrates very fast, and the result may reflect the temperature of sampling rather than the subsurface temperature. The average temperature predicted by the K/Mg geothermometer was 96°C, with a minimum temperature of 67.6°C in water sample GW-117, and a maximum of 106.6°C observed in samples GW-124 and GW-125. Sample GW-181, which belongs to the Mombacho south side region, was included in this plot just to keep in mind another possible type of evidence for waters mixed with deep hot fluid, but will not be used for interpretation in the Granada City region.

As can be seen, the Na/K temperatures were quite similar. It is possible that all the samples are part of the same system and probably in contact with the same shallow water, except for samples GW-117 and GW-181. The temperatures predicted are considerably higher than those predicted by K/Mg; the minimum and maximum temperatures predicted were 174.4 and 303.9°C, respectively. Considering that all these points plotted in the immature water zone, these extremely high results were expected. The Na-K-Ca temperature predictions were very similar to those predicted by K/Mg geothermometers except for water samples GW-131 and GW-144, for which the average, minimum and maximum temperature predicted were 84.7/42.2/105.3°C, respectively. A peculiar result was observed in the prediction for GW-181 in that it was extremely low (57.8°C).

Apoyo Lagoon
A rather different situation was found for Apoyo Lagoon water samples. Again, the K/Mg temperatures were the lowest predicted for every sample, the minimum and maximum temperatures being 69.3°C (GW-103) and 176.3°C (GWI5), respectively, and the average temperature 105.7°C. The Na/K temperatures predicted were not as high as for Granada city, the minimum and maximum temperatures being 80.3°C (MW-71) and 316.2°C (GW-121), respectively, for water samples MW59, GW-83 and GWI5. The difference between the K/Mg and Na/K temperatures predictions is fairly small compared with the Granada city ones, for instance, the K/Mg and Na/K temperature predictions for water sample GW-83 were fairly close. This behaviour is to be expected as this sample plotted directly on the full equilibrium curve. The difference between temperatures predicted for water samples GW-71, GW-78, GW-103, GW-113, GW119 and GW-121 is quite large and can be attributed to lack of equilibrium.

The results for the Na-K-Ca geothermometer in Granada city were quite similar to the K/Mg temperature predictions except for samples GW-59, GW-83 and GWI5, for which predictions were higher than even the temperatures predicted by Na/K geothermometers,

3.3.3 Gas geothermometry

In the Geothermal Master Plan of Nicaragua, three gas samples were reported; two of them were collected at the same place on the same day, the remaining one was contaminated with air, and had a high content of nitrogen (70 %) and oxygen (20 %). The composition of these gas samples can be seen in Table 2 in Appendix I.

To predict the subsurface temperature, the D'Amore and Panichi (1980) gas geothermometer was used. The fumarole sampled is located in the Mombacho volcano region, and the temperature suggested is 394°C. It is possible that another system exists below the Mombacho Volcano, but there is not enough data to conclude on this. The temperatures predicted can be seen in Table 7 in the Appendix I.

3.4 Isotopes

The isotope content (deuterium and oxygen 18) for samples from this area was represented by fifteen water samples collected in several locations. The resulting plot is shown in Figure 9; the data used to construct this plot is presented in Table 3 in Appendix I.

The water samples collected from Apoyo Lagoon plot in the region below the meteoric line. On the $\delta D/\delta^{18}O$ diagram, this shift in the isotope content can be considered as isotope enrichment, and could probably be caused by the *evaporation process that naturally occurs in large bodies of water; during this process, the lighter isotopes of hydrogen and oxygen are the main atoms used to form the molecules of water that escape from the lagoon, so the ratio of ^{18}O and D will increase.* Also, the discharge of deep hot aquifers with shifted isotope ratios of D and ^{18}O can contribute to an increase in the isotope shift, but this factor is negligible if the discharge is compared with the volume of the lagoon. Furthermore, bodies of water are always undergoing a dilution process, mainly caused by the addition of rainwater.

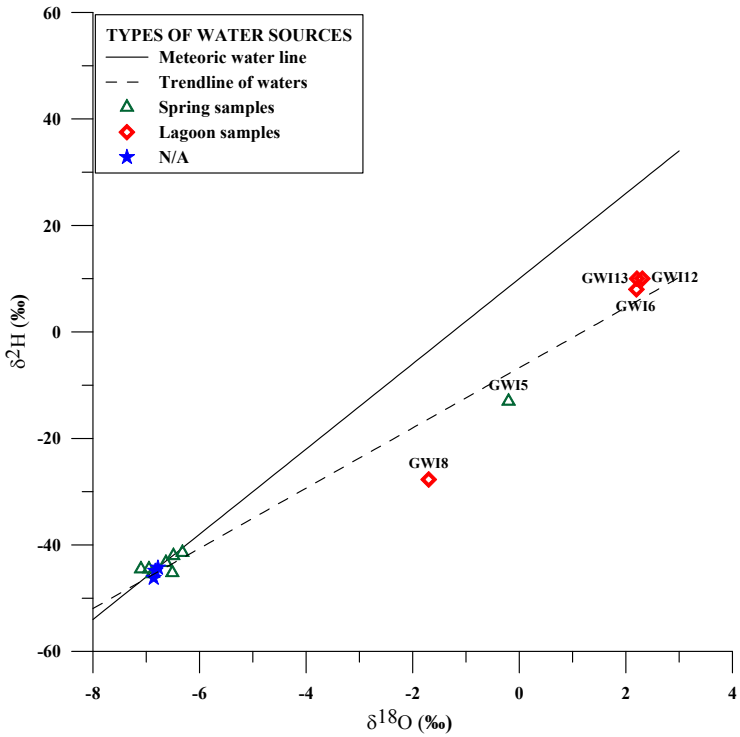

FIGURE 9: Isotope ratios of Masaya-Granada-Nandaime water samples

All spring waters except GWI5 plot directly on the global meteoric water line. This fact clearly suggests that these waters, with the exception of sample GWI5, are meteoric waters that may not necessarily be diluted. The shift in sample GWI5 may be attributed to a deep hot water component which has interacted with minerals along its path.

3.5 Mixing models

The water samples from each region were plotted applying the Schoeller diagram (see Figures 1-7 in Appendix I). To make the analysis easier the ternary plots "HCO_3-Cl-SO_4^{-2}" and "Na-K-Mg" were applied separately for each region (see Figures 1-7 in Appendix I). To estimate the subsurface water temperatures attempts were made to use the "chloride-enthalpy" (Cl-H) and "silica-enthalpy" (SiO_2-H) mixing models.

3.5.1 Chloride-enthalpy model

It turned out that it was not possible to apply this procedure because the water samples were taken from springs located too close to the crater lake for a mixing process to take place; these chloride-rich water samples may simply be reflecting evaporation. Another problem is that there are no cold water samples which can be regarded as end members. For chloride and CO_2 content, it was not possible to evoke a theoretical end member as was done for SiO_2.

3.5.2 Silica-enthalpy model

None of the water samples from Apoyo Lagoon or Granada City were cold ground water samples with silica content of a non-geothermal end-member. To apply this technique, a hypothetical water sample with a silica content of about 17 ppm (according to the chalcedony geothermometer at 25°C, the ambient temperature of the area) was used to represent surface water as a non-geothermal end

member. For the water sample with the highest temperature (GWI5), it was found that the enthalpy and temperature of the deep hot fluid were 605 kJ/kg and 143.5 ºC, respectively (Figure 10). It has to be said that this estimation is not reliable because it did not take into account the contribution of water samples GW-121, GW-103, GW-113, GW-119 and MW-78.

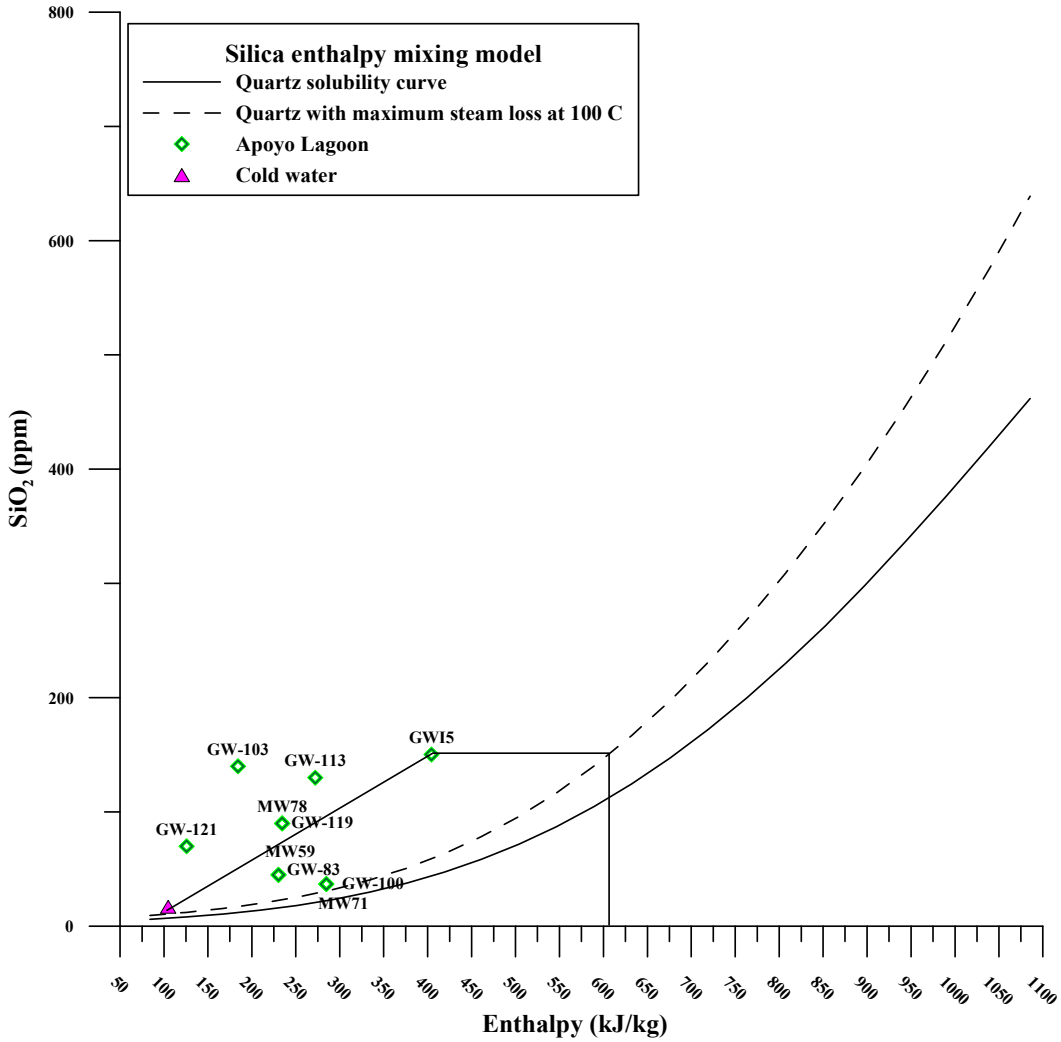

FIGURE 10: SiO_2-enthalpy mixing model for Apoyo Lagoon water samples

3.6 Speciation using WATCH

The speciation technique was applied only to water samples classified as chloride waters according to the HCO_3-Cl-SO_4^{-2} ternary diagram (see Figure 3). The plots for all the saturation index curves for the chloride water samples can be seen in Figures 11 and 12. The following minerals were considered: calcite, quartz, anhydrite, wollastonite and sometimes fluorite (when fluoride content was reported for the water sample). Others minerals showed a saturation index (log Q/K) too high to be considered as useful to study possible equilibria. The first value shown in every plot corresponds to the sampling temperature, except for water sample GWI5 which was sampled at 96.5°C. All the water samples were evaluated at the sampling temperature, and at 50, 100, 150 and 200°C.

All the samples showed calcite supersaturation except water samples GWI5, GW-83 and MW-59. In all the samples, the plots of quartz and fluorite behaved as parallel lines along the whole interval of temperatures, so the minerals that can help to predict a probable equilibrium are anhydrite and

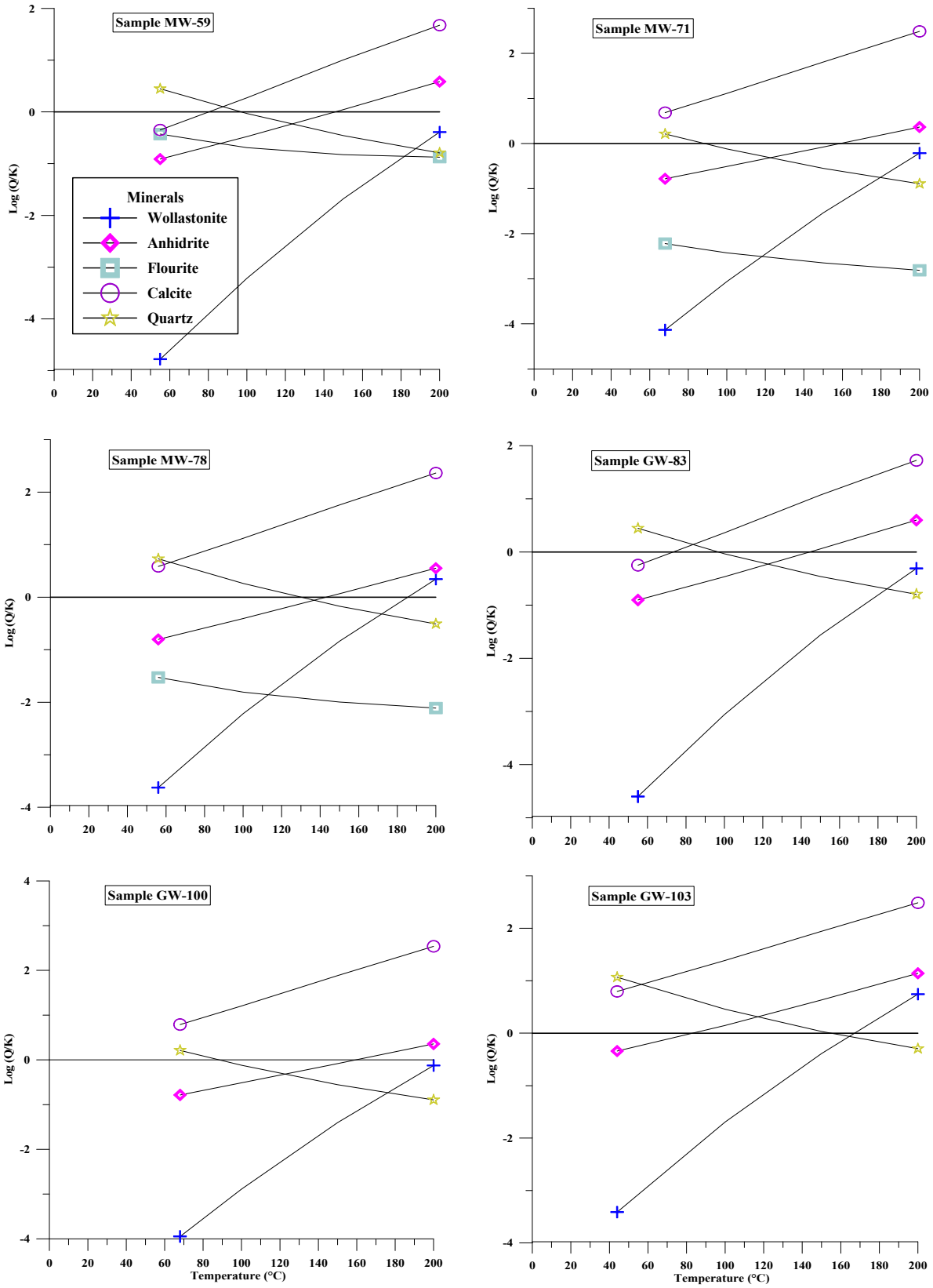

FIGURE 11: SI (log Q/K) curves for Apoyo Lagoon water samples

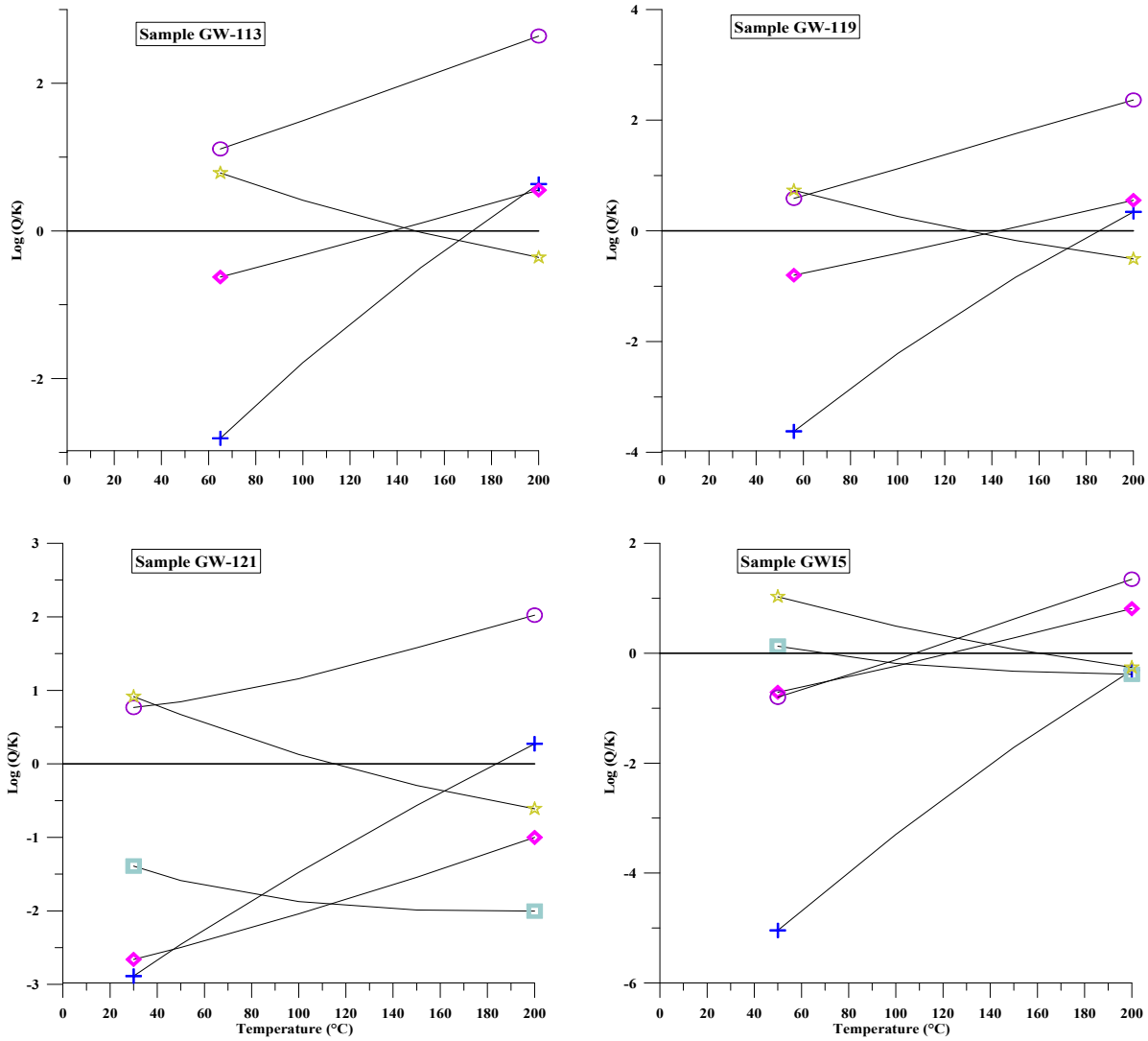

FIGURE 11 cont.: SI (log Q/K) curves for Apoyo Lagoon water samples

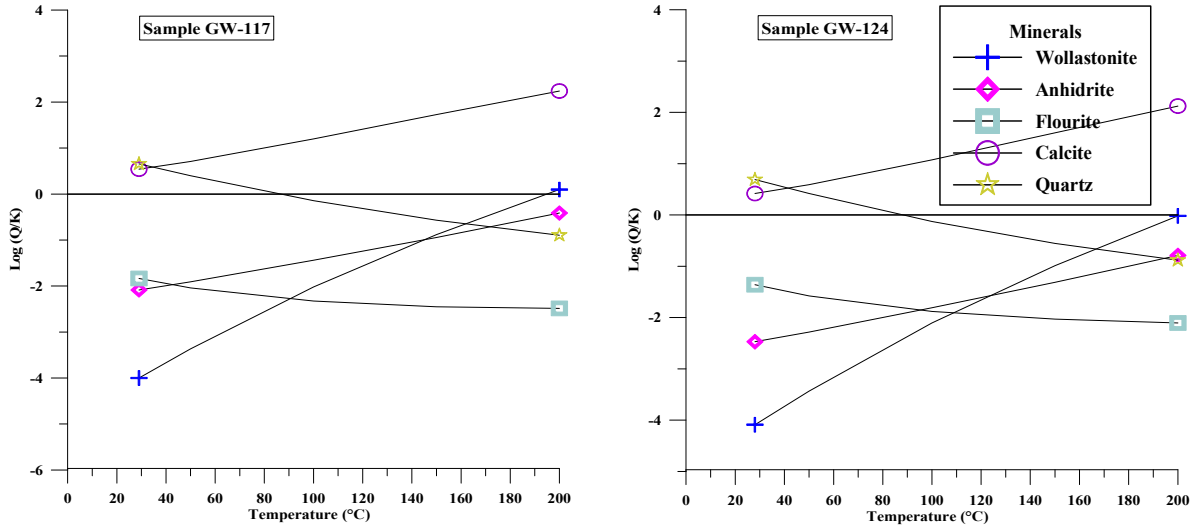

FIGURE 12: SI (log Q/K) curves for Granada City water samples

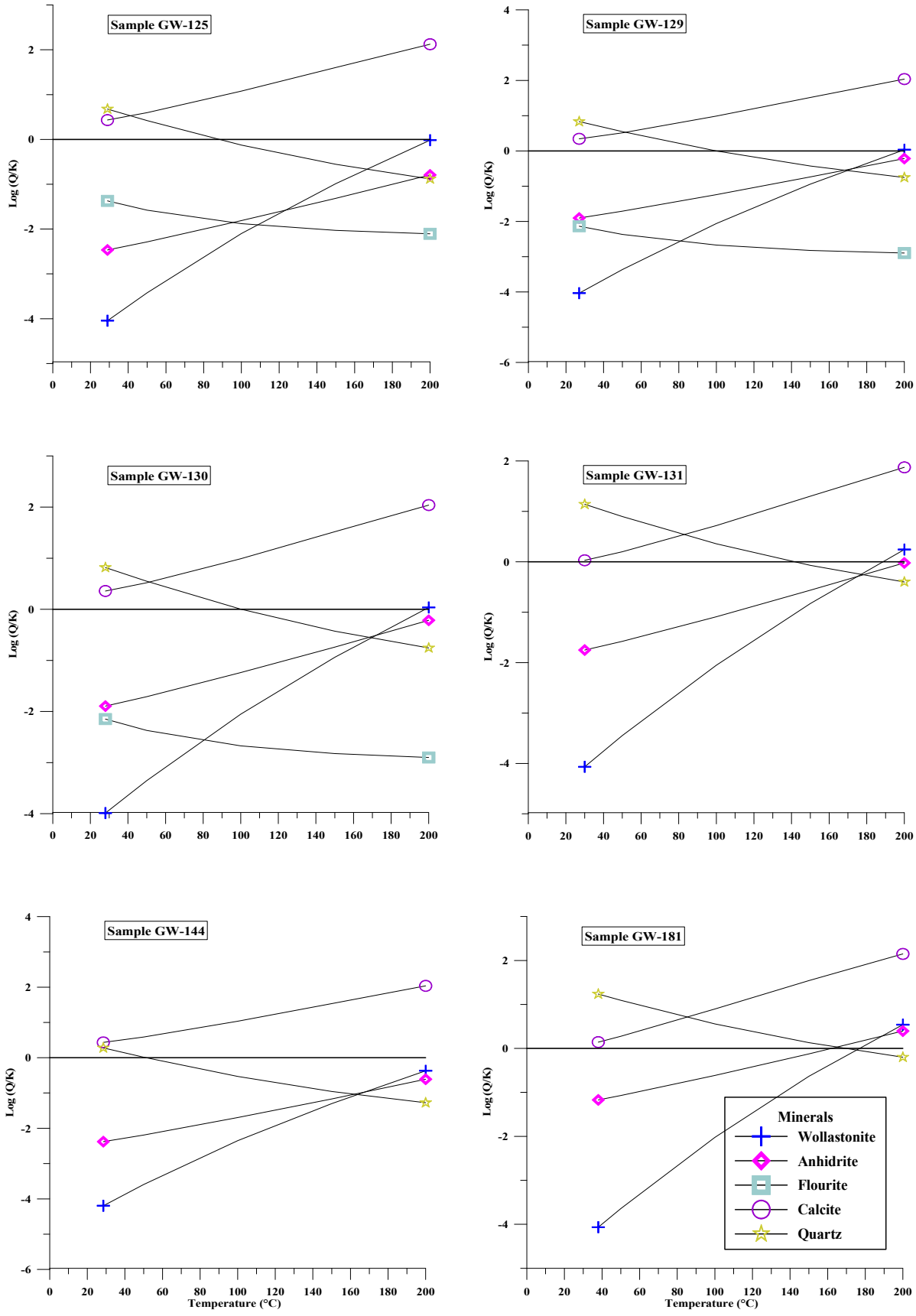

FIGURE 12 cont.: SI (log Q/K) curves for Granada City water samples

wollastonite. Calcite can also be used but the intersection points with calcite always indicate a very low temperature except for sample GWI5. The possibilities of equilibrium are evaluated when at least three SI lines for different minerals intersect each other in a temperature range where the difference is no more than 20°C.

The water samples of Apoyo Lagoon (Figure 11) showed a very scattered pattern, suggesting that they had not attained equilibrium. This can be deduced because the SI lines for the minerals did not intersect the equilibrium line (SI = 0) at the same temperature. This behaviour can possibly be due to boiling, degassing and dilution processes.

In sample MW-59 it is possible to observe two stages of equilibrium that suggest different equilibrium temperatures:

1) In a fairly narrow range (70-100°C) calcite and quartz are almost in equilibrium;
2) Whereas wollastonite and fluorite intersect each other at 180°C and quartz and wollastonite intersect each other at 188°C, so the assemblage wollastonite, fluorite and quartz is in equilibrium in the range 180-188°C.

The problem with the second assumption of equilibrium is that the intersections do not occur on the equilibrium line, but this could be caused by dilution of the deep hot water component with shallow meteoric waters. The second stage of equilibrium was considered to indicate the most likely temperature of the deep hot water component.

The plot for sample GWI5 suggested three different temperature equilibria:

1) The minerals calcite, anhydrite, and fluorite intersect in the range 86-105°C;
2) The minerals calcite, anhydrite and quartz, intersect in the range 108-128°C;
3) The minerals wollastonite, fluorite and quartz, practically converge at 200°C.

It is difficult to state which of these possible equilibria reflects the actual situation.

In Granada City (Figure 12) samples GW-117, GW-129, GW-130, GW-131 GW-144 showed practically the same behaviour. The whole group of samples showed possible dilution with meteoric waters, according to the location of the main intersection point of the minerals. The minerals wollastonite, anhydrite and quartz, intersect each other in narrow bands as follows: GW-117 (148-170°C), GW-129 (158-168°C), GW-130 (158-170°C), GW-131 (170-180°C), GW-144 (152-162°C). As can be noticed, the trend of all the water samples points to a possible deep hot water temperature in the range 150-170°C.

For sample GW-181, from the south side of Mombacho volcano, the minerals quartz, wollastonite and anhydrite also intersected in a narrow band between 155 and 175°C. This is practically on the equilibrium line, suggesting that these minerals have more or less attained equilibrium with water, and the deep hot water temperature could be in the range 150-170°C.

4. CONCLUSIONS AND RECOMMENDATIONS

4.1 Conclusions

Geochemical techniques have been applied to evaluate chemical data from the potential geothermal area of Masaya-Granada-Nandaime.

- The water samples from the Apoyo Lagoon and Granada City region showed signs of mixing of geothermal waters and cold groundwater.
- Taking into account the classification of the samples according to the ternary diagram (HCO_3-Cl-SO_4), it was possible to deduce that the samples with higher Cl, Na, K, lower Mg content, and near neutral pH, pointed to a zone with high permeability and direct communication with a deep hot water source (Apoyo Lagoon water samples). Steam heated waters, sulphate waters and bicarbonate waters were usually located around the heat source (Mombacho north side, Mombacho volcano and Mombacho south side), so it is possible to predict the existence of a geothermal system centred in the Apoyo Lagoon region. The water samples from the other regions were mainly composed of cold surface waters.
- The most common geothermometers were applied and comparable temperatures were predicted. Quartz, K/Mg and Na-K-Ca geothermometers showed results that were reasonably close; the average temperatures predicted for Apoyo Lagoon and Granada City when applying these techniques are as follows:
  - Apoyo Lagoon silica/cation geothermometry yields 94/90°C;
  - Granada City silica/cation geothermometry yields 111/115°C.
- The plotting of water samples in the Na-K-Mg ternary diagram suggests that just a few water samples have attained equilibrium between K-feldspars and Na-feldspars, therefore the Na/K temperature predictions could be too high and not representative of the actual deep hot water temperature.
- The gas geothermometer predictions indicate high temperatures under Mombacho volcano, but the samples are only two, and both are from the same place.
- Sample GWI5 shows a deep hot water component with respect to the isotope results.
- The temperatures predicted with log (Q/K) were not comparable for Apoyo Lagoon water samples. On the other hand, the log (Q/K) worked well for Granada City water samples; the mineral assemblage indicates that equilibrium has been attained in the range 150-170°C.

4.2 Recommendations

Considering the problems found in the evaluation of the available chemical data taken from Masaya-Granada-Nandaime area, it is necessary to carry out the following activities:

- Conduct a new geochemical sampling in the Masaya-Granada-Nandaime area according to the guidelines presented by Arnórsson, et al. (2006) and Ármannsson and Ólafsson (2006).
- Analyse the water samples according to the guidelines presented by Pang and Ármannsson (2006).
- Determine the trace metal content in the water samples.
- Carry out a sampling campaign around the entire Apoyo Lagoon region.
- Carry out a sampling campaign in the Mombacho Volcano fumaroles.

ACKNOWLEDGEMENTS

I would like to give thanks to Ruth and Francisco, my dear parents, to Myriam and my children, to Dr. Ármannsson (my advisor) and Dr. Bjarnason for their invaluable help. Also I would like to thank Mrs. Magdalena Perez, who has been supportive of me during all this time and the very kind staff of the UNU-GTP. Finally I would like to thank God for allowing me to take this chance to improve my knowledge

REFERENCES

Ármannsson, H., and Ólafsson, M., 2006: *Collection of geothermal fluids for chemical analysis.* ÍSOR, report ISOR-2006/016, 17 pp.

Arnórsson, S., 1987: Gas chemistry of the Krísuvík geothermal field, Iceland, with special reference to evaluation of steam condensation in upflow zones. *Jökull, 37*, 31–47.

Arnórsson, S. (ed.), 2000: *Isotopic and chemical techniques in geothermal exploration, development and use. Sampling methods, data handling, interpretation.* International Atomic Energy Agency, Vienna, 351 pp.

Arnórsson, S., Andrésdóttir, A., Gunnarsson, I., and Stefánsson, A., 1998: New calibration for the quartz and Na/K geothermometers – valid in the range 0-350°C (in Icelandic). *Proceedings of the Geoscience Society of Iceland Annual Meeting, April,* 42-43.

Arnórsson, S., and Bjarnason, J.Ö., 1993: *Icelandic Water Chemistry Group presents the chemical speciation program WATCH.* Science Institute, University of Iceland, Orkustofnun, Reykjavík, 7 pp.

Arnórsson, S., Bjarnason, J.Ö., Giroud, N., Gunnarsson, I., and Stefánsson, A., 2006: Sampling and analysis of geothermal fluids. *Geofluids, 6,* 203-216.

Arnórsson, S., Björnsson, S., Muna, Z.W., and Bwire-Ojiambo, S., 1990: The use of gas chemistry to evaluate boiling processes and initial steam fractions in geothermal reservoirs with an example from the Olkaria field, Kenya. *Geothermics, 19-6,* 497-514.

Arnórsson, S., Gunnlaugsson, E., and Svavarsson, H., 1983: The chemistry of geothermal waters in Iceland III. Chemical geothermometry in geothermal investigations. *Geochim. Cosmochim. Acta, 47*, 567-577.

Arnórsson, S., Sigurdsson, S. and Svavarsson, H., 1982: The chemistry of geothermal waters in Iceland I. Calculation of aqueous speciation from 0°C to 370°C. *Geochim. Cosmochim. Acta, 46,* 1513-1532.

CNE, 2001: *Nicaragua geothermal master plan.* National Energy Commission of Nicaragua (CNE) and Geothermex, report, vol. X, 28 pp.

Craig, H., 1961: Isotopic variations in meteoric water. *Science, 133*, 1702-1703.

Craig, H., 1963: The isotopic geochemistry of water and carbon in geothermal areas. In: Tongiorgi, E. (ed.), *Nuclear geology on geothermal areas*. Consiglio Nazionale delle Ricerche, Laboratorio di Geologia Nucleare, Pisa, 17-53.

Craig, H., Boato, G., and White, D.E., 1956: Isotope geochemistry of thermal waters. In: *Proceedings of the 2nd Conference on Nuclear Processes in Geologic Settings, National Academy of Sciences-National Research Council,* paper 400, 29-38.

D´Amore, F., and Panichi, C., 1980: Evaluation of deep temperatures in a geothermal system by a new geothermometer. *Geochim. Cosmochim. Acta, 44,* 549-556.

D'Amore, F., and Truesdell, A.H., 1985: Calculation of geothermal reservoir temperatures and steam fraction from gas compositions. *Geoth. Res. Council, Trans., 9,* 305-310.

Ellis, A.J., and Mahon, W.A.J., 1964: Natural hydrothermal systems and experimental hot-water/rock interactions. *Geochim. Cosmochim. Acta, 28,* 1323-1357.

Ellis, A.J., and Mahon, W.A.J., 1967: Natural hydrothermal systems and experimental hot water/rock interactions (part II). *Geochim. Cosmochim. Acta, 31*, 519-538.

Ellis, A.J., and Wilson, S.H., 1960: The geochemistry of alkali metals ions in the Wairakei hydrothermal system. *N.Z.J. Geol. & Geophys., 3*, 593-617.

Fournier, R.O., 1977: Chemical geothermometers and mixing models for geothermal systems, *Geothermics, 5,* 41-50.

Fournier, R.O., 1979: A revised equation for Na-K geothermometer. *Geoth. Res. Council, Trans., 3,* 221-224.

Fournier, R.O., 1989: *Lectures on geochemical interpretation of hydrothermal waters.* UNU-GTP, Iceland, report 10, 73 pp.

Fournier, R.O., and Potter, R.W. II, 1982: A revised and expanded silica (quartz) geothermometer. *Geoth. Res. Council Bull.,11-10*, 3-12.

Fournier, R.O., and Truesdell, A.H., 1973: An empirical Na-K-Ca geothermometer for natural waters. *Geochim. Cosmochim. Acta*, *37*, 1255-1275.

Giggenbach, W.F., 1988: Geothermal solute equilibria. Derivation of Na-K-Mg-Ca geoindicators. *Geochim. Cosmochim. Acta, 52*, 2749-2765.

Giggenbach. W.F., 1991: Chemical techniques of geothermal exploration. In: D'Amore, F (coordinator), *Applications of geochemistry in geothermal reservoir development*. Unitar/UNDP publication, Rome, 119-142.

Hem, J.D., 1970: *Study and interpretation of the chemical characteristics of natural water* (2nd edition). U.S. Geological Survey, water-supply paper 1473, 363 pp.

INETER, 1997: *Annual report* (in Spanish). INETER, Managua.

Mahon, W.A.J., Klyen, L.E., and Rhode, M., 1980: Neutral sodium/bicarbonate/sulphate hot waters in geothermal systems. *Chinetsu (J. Japan Geothermal Energy Association), 17,* 11-24.

Nicholson, K., 1993: *Geothermal fluids: chemistry and exploration techniques*. Springer-Verlag, Berlin, 268 pp.

Nieva, D., and Nieva, R., 1987: Developments in geothermal energy in Mexico, part 12-A: Cationic composition geothermometer for prospection of geothermal resources. *Heat Recovery Systems and CHP, 7,* 243-258.

Nuti, S., 1991: Isotope techniques in geothermal studies. In: D´Amore, F. (coordinator), *Applications of geochemistry in geothermal reservoir development.* UNITAR/UNDP publication, Rome, 215-251.

Pang Z., and Ármannsson, H. 2006: *Analytical procedures and quality assurance for geothermal water chemistry.* UNU-GTP, Iceland, report 1, 172 pp.

Reed, M.J., and Mariner, R.H., 1991: Quality control of chemical and isotopic analyses of geothermal water samples. *Proceedings of the 16th Workshop on Geothermal Reservoir Engineering, Stanford University, Stanford, Ca,* 9-13.

Reed, M.H., and Spycher, N.F., 1984: Calculation of pH and mineral equilibria in hydrothermal water with application to geothermometry and studies of boiling and dilution. *Geochim. Cosmochim. Acta, 48*, 1479-1490.

Tonani, F., 1980: Some remarks on the application of geochemical techniques in geothermal exploration. *Proceedings, Adv. Eur. Geoth. Res., 2nd Symposium, Strasbourg*, 428-443.

Truesdell, A.H., 1991: Effects of physical process on geothermal fluids. In: D'Amore, F. (Coordinator), *Applications of geochemistry in geothermal reservoir development*. Unitar/UNDP publication, Rome, 71-92.

Truesdell, A.H., and Fournier, R.O., 1976: Calculations of deep temperatures in geothermal systems from the chemistry of boiling spring waters of mixed origin. *Proceedings of 2nd U.N. Symposium on the Development and Use of Geothermal Resources, San Francisco, 1,* 837-844.

APPENDIX I: Chemical data, location of sampling points and interpretation

TABLE 1: Chemical data of the Masaya-Granada-Nandaime geothermal area (concentrations in ppm)

ID	utm-E	utm-N	Temp. (°C)	pH	Alc(HCO3)	HCO_3	CO_3	Cl	SO_4	Na	Ca	Mg	K	F	B	SiO2	Ionic balance (%)
Masaya																	
MW25	593.4	1311.7	27	8	2.63	160.15	0.72	10.99	0.00	16.09	28.06	8.15	7.04	0.00	N/A	54	-0.28
MW66	586.2	1316.3	27	7.8	3.17	193.40	0.55	8.51	7.21	30.03	22.04	10.35	9.00	N/A	N/A	N/A	-2.57
MW77	596	1318.5	25	7.8	3.07	187.42	0.52	4.61	1.68	25.41	24.05	9.74	8.60	N/A	0.37	N/A	2.20
MW83	595.3	1322.6	29	8.5	4.40	268.49	3.99	6.03	3.99	57.75	12.02	14.61	17.60	N/A	0.02	N/A	-0.49
MW85	607.3	1323.2	28	7.9	3.77	230.23	0.84	14.00	2.00	53.00	28.00	6.00	10.00	0.30	0.00	39	4.91
MW110	591.1	1331.7	38	7.7	13.35	814.54	2.13	28.01	76.85	110.35	58.12	93.63	23.85	N/A	0.86	86	1.27
MW112	589.2	1334.7	27	7.4	3.00	183.19	0.20	20.92	27.86	68.97	14.03	5.96	5.87	N/A	0.11	51	3.78
Granada City																	
GW-104	614.5	1316.9	30	7.5	152.55	141.15	0.20	15.95	12.01	20.00	30.06	7.05	6.26	N/A	0.11	101	2.93
MW114	612	1331.2	27	8.1	268.49	261.96	1.49	13.83	10.09	75.87	20.04	5.23	16.03	N/A	0.11	73	3.90
GW-117	612.4	1318.9	29	7.9	220.28	213.13	0.80	283.6	28.82	170.82	60.12	16.17	23.46	0.30	1.30	36	1.97
GW-124	611.0	1319.7	28	8	256.27	249.16	1.15	400.59	22.09	287.83	34.07	11.19	38.32	0.70	1.80	38	1.50
GW-125	610.8	1319.9	29	8	256.09	249.01	1.17	401.00	22.00	288.00	34.00	11.00	38.40	0.70	1.80	38	1.38
GW-129	610.9	1320.5	27	8	237.95	231.31	1.05	690.92	99.90	480.72	36.07	16.17	62.17	0.30	2.40	51	0.92
GW-130	610.8	1320.7	28	8	238.18	231.57	1.07	692.00	100.00	481.00	36.00	16.00	62.00	0.30	2.40	51	0.74
GW-131	610.6	1320.8	30	7.7	189.16	180.96	0.48	496.3	124.88	344.85	34.07	12.04	50.83	N/A	6.05	113	-3.06
GW-144	610.7	1322.6	29	8.1	164.75	160.76	0.94	166.62	20.17	120.01	36.07	9.73	10.56	N/A	0.15	15	3.84
GW-145	610.4	1322.9	29	8.1	176.88	172.60	1.02	167.00	20.00	120.00	36.00	9.60	10.40	0.20	0.15	15	1.02
GW-152	613.1	1325	27	7.7	158.65	151.48	0.37	70.90	11.05	41.38	38.08	10.94	7.82	N/A	0.08	94	1.58
Apoyo Lagoon																	
MW59	603.8	1315.9	55	7	152.50	126.16	0.08	2023.50	400.00	1412.00	90.00	12.00	44.00	2.30	4.00	45	0.81
MW71	602.8	1317.8	68	7.1	738.00	631.96	0.57	1420.00	350.00	1174.00	110.00	25.2	32.00	0.30	14.00	37	2.95
MW78	603.4	1319.2	56	7.4	415.00	382.67	0.64	1420.00	420.00	1080.00	104.00	20.00	65.00	0.60	5.00	90	0.69
GW-83	603.8	1315.6	55	7	151.94	125.69	0.08	2020.30	400.09	1411.40	90.18	4.62	44.18	N/A	4.00	45	0.03
GW-100	602.9	1316.8	68	7.1	738.34	632.25	0.57	1418.00	350.14	1173.40	110.22	25.54	32.06	N/A	14.00	37	3.06
GW-103	602.7	1316.9	44	7.4	329.51	303.21	0.45	602.65	528.33	298.87	280.56	47.42	25.02	N/A	7.03	140	-4.47
GW-113	602.8	1318	65	7.6	671.22	634.62	1.71	1382.60	480.30	1103.50	130.26	30.40	82.11	N/A	16.22	130	-0.60
GW-119	603.1	1319.1	56	7.4	414.94	382.61	0.64	1418.00	420.26	1079.60	104.21	20.31	65.30	0.00	5.00	90	0.84
GW-121	603.1	1319.4	30	8.4	170.45	166.85	2.01	1292.00	12.00	715.00	62.00	28.00	115.00	0.60	4.30	70	-0.14
GWI5	603.4	1316.3	97	6.7	142.00	93.003	0.03	2250.00	664.00	1603.30	110.09	2.00	175.44	4.00	26.64	150	1.35
Mombacho north side																	
GW-41	615.1	1310.9	36	7.2	140.00	122.60	0.10	14.00	280.00	30.00	94.00	31.00	3.00	1.00	5.00	39	4.57
GW-42	615.1	1310.9	54	7.2	373.00	329.35	0.34	180.00	96.00	160.00	88.00	10.00	33.00	0.30	0.20	180	4.17
GW-47	614.9	1311	36	6.9	128.13	99.95	0.04	6.38	528.34	30.03	198.40	24.35	4.69	N/A	0.08	198	3.90
GW-54	617.4	1311.7	54	7.2	341.71	297.54	0.28	131.17	220.94	140.24	82.16	27.97	25.81	N/A	2.59	190	-0.19
GW-56	617.3	1311.8	54	7.2	372.22	328.66	0.34	180.09	96.06	160.01	88.18	9.73	33.24	0.38	0.20	180	4.18
GWI2	614.9	1310.9	38	7.6	126.00	119.38	0.27	5.07	469.00	28.40	175.00	22.60	5.25	0.71	0.00	115	0.74
GWI3	617.3	1311.8	54	7.4	352.00	326.67	0.59	143.00	222.00	152.00	88.40	26.80	27.10	0.39	1.59	200	-0.78

TABLE 1: Continued

ID	utm-E	utm-N	Temp. (°C)	pH	Alc(HCO3)	HCO_3	CO_3	Cl	SO_4	Na	Ca	Mg	K	F	B	SiO2	Ionic Balance (%)
Mombacho Volcano																	
GW-9	611.8	1305.2	49	7.8	262.39	253.41	1.07	9.93	1008.60	119.55	280.56	70.53	26.98	N/A	0.11	160	0.87
GW-14	611.8	1306.1	26	7.3	73.22	65.21	0.06	95.72	230.06	45.06	88.18	28.33	5.08	0.80	0.35	83	3.00
GW-22	612.4	1306.9	30	7.9	97.63	94.48	0.36	18.08	211.33	42.76	60.12	18.24	8.21	N/A	N/A	37	1.54
GW-26	612.8	1307.2	43	7.7	84.82	81.10	0.24	31.91	134.96	29.89	52.10	14.23	3.91	1.10	0.18	100	2.42
GW-32	613.0	1307.5	36	7.5	98.24	91.61	0.15	88.98	119.11	51.96	62.12	14.23	5.08	1.00	0.45	110	2.50
GW-208	620.4	1302.9	31	7.6	85.43	80.57	0.16	24.82	11.05	20.92	10.02	9.73	2.74	N/A	N/A	30	1.09
GW-212	620.3	1303	31	7.6	85.40	80.54	0.16	25.00	11.00	21.00	10.00	9.60	2.70	0.30	0.00	30	0.52
GW-226	611.6	1306.1	26	7.3	73.00	65.02	0.06	96.00	230.00	45.00	88.00	28.00	5.00	0.80	0.35	80	2.49
GW-228	612.2	1306.7	31	7.9	73.00	70.66	0.27	36.00	135.00	38.00	40.00	16.00	5.00	0.80	0.12	86	1.98
GW-229	611.9	1306.9	45	7.8	104.00	100.23	0.38	14.20	192.00	42.00	54.00	18.00	8.00	0.70	0.10	40	2.51
GW-230	611.7	1307.3	30	7.9	97.60	94.50	0.36	18.00	211.00	42.70	60.00	18.00	8.00	0.60	0.00	37	1.17
GW-231	611.7	1307.6	43	7.7	85.00	81.27	0.24	32.00	135.00	30.00	52.00	14.00	4.00	1.10	0.18	100	1.97
GWI1	612.2	1307.3	47	7.4	144.00	131.64	0.18	8.34	231.00	33.00	80.20	18.10	12.50	1.03	0.00	144	0.52
Mombacho south side																	
GW-156	619.4	1291.6	27	7.7	378.32	360.18	0.82	98.91	0.00	48.97	90.18	28.33	5.47	0.30	0.10	54	4.26
GW-157	619.3	1291.7	27	7.7	378.00	359.88	0.82	99.00	0.00	48.90	90.00	28.00	5.50	0.30	0.10	54	3.87
GW-163	609.5	1292.5	29	7.7	299.00	284.88	0.67	102.81	1.44	56.79	72.14	20.31	3.13	0.30	0.05	53	2.58
GW-169	611.2	1299.1	27	7.6	580.30	546.25	0.98	180.80	10.09	88.28	88.18	75.03	14.47	0.10	0.00	30	3.35
GW-170	610.9	1299.1	27	7.6	580.00	545.97	0.98	181.00	10.00	88.40	88.00	74.00	14.40	0.10	0.00	30	2.75
GW-171	613.3	1300.8	29	8.4	316.72	310.08	3.66	25.00	48.00	11.00	66.00	37.00	4.00	0.60	0.80	30	0.14
GW-173	613.6	1300.8	29	8.4	316.60	309.96	3.66	24.82	48.03	11.04	66.13	37.45	3.91	0.60	0.80	30	0.85
GW-181	614.8	1301.4	38	7.4	250.18	227.47	0.28	269.42	192.12	170.13	76.15	32.83	30.11	N/A	2.49	175	-4.44
GW-185	615	1301.5	45	7.7	458.00	438.03	1.32	291.00	220.00	277.50	82.00	42.00	25.90	0.20	0.35	44	1.33
GW-187	614.1	1301.5	45	7.2	256.00	225.45	0.21	126.00	168.00	55.00	92.00	36.00	43.00	0.50	1.15	120	2.67
GW-190	615.8	1301.75	45	7.7	458.26	438.27	1.32	290.69	219.98	277.49	82.16	42.56	25.81	N/A	0.35	44	1.61
GW-196	611	1302	27	7.0	91.53	74.70	0.04	8.86	360.23	32.19	110.22	25.54	14.08	N/A	0.08	98	4.21
GW-198	613.9	1302	55	7.4	280.69	260.10	0.46	209.16	398.65	200.01	110.22	42.56	50.83	N/A	3.03	200	2.79
GW-199	610.1	1302.1	36	7.5	98.00	91.38	0.15	89.00	119.00	52.00	62.00	14.00	5.00	1.00	0.45	110	2.20
GW-200	612.6	1302.2	27	8	225.77	219.47	0.99	21.27	389.04	54.72	124.25	44.99	12.12	N/A	0.05	28	2.10
GW-201	612.3	1302.3	27	8	226.00	219.70	1.00	21.30	389.00	54.70	124.00	44.40	12.00	0.90	0.05	28	1.55
GW-219	611.2	1303.2	24	8	85.42	83.00	0.35	8.86	427.47	34.65	128.26	28.00	8.21	N/A	N/A	102	-0.97
Nandaime																	
NW-4	582.2	1291.8	28	8.1	226.00	220.52	1.28	21.30	48.00	63.70	38.00	8.40	1.60	0.10	0.55	18	2.66
NW-5	582.2	1291.9	28	8.1	225.77	220.29	1.28	21.27	48.03	63.68	38.08	8.51	1.56	N/A	0.55	18	2.94
NW-6	590.7	1292.8	25	8.0	390.00	379.18	1.69	18.00	50.00	130.00	28.00	13.00	1.00	0.00	0.00	18	4.09
NW-8	591	1294.4	27	7.7	195.20	185.84	0.42	28.40	4.00	18.00	14.00	30.00	5.00	0.10	0.10	21	3.33
NW-9	591.1	1294.6	27	7.7	195.26	185.86	0.42	28.36	3.84	17.93	14.03	30.40	5.08	N/A	0.10	21	4.25
NW-25	604.3	1297.5	25	7.8	336.00	323.04	0.93	25.00	10.00	74.00	43.00	11.00	10.00	0.00	0.00	40	4.48
NW-45	584.9	1300.8	27	8.1	238.00	232.21	1.32	18.00	4.00	28.5	34.00	18.00	4.40	0.00	0.25	32	1.97
NW-46	584.9	1300.8	27	8.1	237.98	232.19	1.32	18.08	3.84	28.51	34.07	18.24	4.30	N/A	0.25	32	2.47
NW-57	603.6	1302.2	25	7.8	183.00	175.94	0.51	11.00	5.00	32.00	20.00	11.00	5.00	0.20	0.00	5	3.20
NW-103	591.5.	1304.6	25	7.8	159.00	152.98	0.45	11.00	2.00	25.00	20.00	10.00	4.00	0.20	0.00	43	4.62

TABLE 2: Gas data for the Masaya-Granada-Nandaime geothermal area (concentrations in volume percentage)

ID	utm-E	utm-N	CO_2	H_2S	NH_3	Ar	N_2	CH_4	H_2	He	O_2	Sum
GG1	611,8	1307,5	9,8	0			69,50	0	0,2		20	99
GG2	611,7	1307,9	73,3	9,62	0	0	0,14	0	16,9	0	0	100
GW35	611,7	1307,9	73,4	9,48	0	0	0,15	0	17	0	0	100

TABLE 3: Isotope data for Masaya-Granada-Nandaime geothermal area

ID	utm-E	utm-N	Type	T (°C)	pH	δ-D(liq)	δ-^{18}O(liq)
GWI1	612.18	1307.31	Spring	46.7	7.36	-41.4	-6.32
GWI2	614.92	1310.93	Spring	37.5	7.62	-44.5	-7.10
GWI3	617.33	1311.83	Spring	53.5	7.44	-43.3	-6.63
GWI4	609.50	1314.75	N/A	28.0	7.47	-44.9	-6.83
GWI5	603.40	1316.3	Spring	96.5	6.67	-13.0	-0.20
GWI6	603.40	1316.3	Lagoon	N/A	7.99	8.0	2.20
GWI7	613.20	1300.75	Spring	30.1	6.92	-45.4	-6.89
GWI8	613.30	1300.80	Lagoon	33.0	7.45	-27.7	-1.70
GWI9	613.50	1300.90	Spring	42.4	6.70	-45.2	-6.51
GWI10	614.90	1301.50	Spring	47.0	7.04	-42	-6.49
GWI11	616.15	1303.10	Spring	28.0	6.64	-44.5	-6.95
GWI12	N/A	N/A	Lagoon	30.0	8.17	10.0	2.31
GWI13	N/A	N/A	Lagoon	30.0	8.31	10.0	2.21
MWI1	607.95	1311.50	N/A	29.0	7.73	-44.3	-6.78
MWI4	606.50	1310.45	N/A	26.0	7.97	-46.2	-6.86

N/A: not available

TABLE 4: List of geothermometers applied

Code	Equation	Reference
Quartz		
Q1	$T(°C)=\frac{1309}{5.19-\log S}-273.15$	Fournier (1977)
Q2[1)]	$T(°C)=\frac{1522}{5.75-\log S}-273.15$	Fournier (1977)
Q3	$T(°C)= -42.2 + 0.28831\times S - 3.6686\times10^{-4}*S^2 + 3.1665\times10^{-7}*S^3 + 77.034\times\log S$	Fournier and Potter (1982)
Q4[1)]	$T(°C)= -53.5 + 0.11236\times S - 0.5559\times10^{-4}*S^2 + 0.1772\times10^{-7}*S^3 + 88.390\times\log S$	Fournier and Potter (1982)
Q5	$T(°C)= -55.3 + 0.3659\times S - 5.3954\times10^{-4}*S^2 + 5.5132\times10^{-7}\times S^3 + 74.360\times\log S$	Arnórsson et al. 1998
Q6[1)]	$T(°C)=- 66.9 + 0.1378\times S - 4.9727\times10^{-5}*S^2 + 1.0468\times10^{-8}*S^3 + 87.841\times\log S$	Arnórsson et al. 1998
Chalcedony		
Ch1	$T(°C)=\frac{1032}{4.69-\log S}-273.15$	Fournier (1977)
Ch2	$T(°C)=\frac{1112}{4.91-\log S}-273.15$	Arnórsson et al. (1983)

Code	Equation	Reference
Na/K		
Na1	$T(°C)=\frac{856}{0.857-\log\left(\frac{Na}{K}\right)}-273.15$	Truesdell and Fournier, 1976
Na2	$T(°C)=\frac{1217}{1.438-\log\left(\frac{Na}{K}\right)}-273.15$	Fournier 1979
Na3	$T(°C)=\frac{833}{0.780-\log\left(\frac{Na}{K}\right)}-273.15$	Tonani 1980
Na4[2)]	$T(°C)=\frac{933}{0.993-\log\left(\frac{Na}{K}\right)}-273.15$	Arnórsson et al. (1983)
Na5[3)]	$T(°C)=\frac{1319}{1.699-\log\left(\frac{Na}{K}\right)}-273.15$	Arnórsson et al. (1983)
Na6	$T(°C)=\frac{1178}{1.470-\log\left(\frac{Na}{K}\right)}-273.15$	Nieva and Nieva 1987
Na7	$T(°C)=\frac{1390}{1.750-\log\left(\frac{Na}{K}\right)}-273.15$	Giggenbach. 1988
Na8	$T(°C)=733.6-770.551\times\log\left(\frac{Na}{K}\right)+378.189\times\log^2\left(\frac{Na}{K}\right)-95.753\times\log^3\left(\frac{Na}{K}\right)+9.544\times\log^4\left(\frac{Na}{K}\right)$	Arnórsson et al. (1998)
K^2/Mg		
K1	$T(°C)=\frac{4410}{14.0-\log\left(\frac{K^2}{Mg}\right)}-273.15$	Giggenbach, (1988)
Gas		
G1	$T(ºC)=\frac{24775}{2\log\left(\frac{CH_4}{CO_2}\right)-6\mathrm{Log}\left(\frac{H_2}{CO_2}\right)-3\log\left(\frac{H_2S}{CO_2}\right)+7\log P(CO_2)+36.05}-273.15$ If $CO_2 < 75$ % then $P(CO_2) = 0.1$ atm If $CO_2 > 75$ % then $P(CO_2) = 1$ atm If $CO_2 > 75$ % and $CH_4 > 2H_2$ and $H_2S > H_2$ then $P(CO_2) = 10$ atm	D`Amore and Panichi (1980)
Na-K-Ca[4)]	$T(°C)=\frac{1647}{\log\left(\frac{Na}{K}\right)+\beta\log\left(\frac{Ca^{0.5}}{Na}\right)+2.74}-273.15$	Fournier and Truesdell (1973)

[1)] After adiabatic boiling to 100°C; [2)] For 25-250°C; [3)] For 250-350°C;
[4)] Concentrations in mole/kg, $\beta = 4/3$ for $t<100°C$; and $\beta = 1/3$ for $t>100°C$ and for $\log(Ca^{0.5}/Na)<0$.

TABLE 5: Quartz and chalcedony temperature predictions for chloride waters (ºC)

ID	Quartz						Chalcedony	
	Q1	Q2	Q3	Q4	Q5	Q6	Ch1	Ch2
Granada city								
GW-117	78.0	89.8	87.6	88.0	72.9	74.7	56.2	58.4
GW-124	76.6	91.8	89.9	90.3	75.3	77.0	58.7	60.8
GW-125	78.0	91.8	89.9	90.3	75.3	77.0	58.7	60.8
GW-129	75.1	103.4	103.1	103.0	89.0	90.0	72.9	74.1
GW-130	76.6	103.4	103.1	103.0	89.0	90.0	72.9	74.1
GW-131	79.4	138.5	144.3	140.0	132.6	128.4	118.2	116.1
GW-144	77.3	59.6	52.6	52.1	37.5	38.5	20.5	24.7
Mombacho South Side								
GW-181	171.0	160.8	171.5	162.8	161.9	152.8	148.6	143.8
Apoyo Lagoon area								
MW59	106.3	98.4	97.4	97.6	83.1	84.4	66.7	68.3
MW71	116.7	90.8	88.8	89.2	74.1	75.9	57.4	59.6
MW78	107.2	127.8	131.6	128.9	119.0	116.8	104.1	103.1
GW-83	106.3	98.4	97.4	97.6	83.1	84.4	66.7	68.3
GW-100	116.7	90.8	88.8	89.2	74.1	75.9	57.4	59.6
GW-103	95.9	149.2	157.2	150.9	146.4	140.0	132.5	129.2
GW-113	114.5	145.4	152.6	147.1	141.6	135.9	127.5	124.6
GW-119	107.2	127.8	131.6	128.9	119.0	116.8	104.1	103.1
GW-121	79.4	116.6	118.4	117.2	105.1	104.6	89.6	89.7
GWI5	135.2	152.8	161.6	154.6	151.2	143.9	137.5	133.7

TABLE 6: Cation temperature predictions for chloride waters (ºC)

ID	K/Mg	Na/K								Na-K-Ca
	K1	Na1	Na3	Na6	Na5	Na4	Na2	Na7	Na8	
Granada city										
GW-117	67.6	174.4	180.7	193.3	205.7	211.6	214.9	222.3	240.9	84.0
GW-124	106.4	216.9	225.7	226.1	236.4	254.3	249.7	253.4	285.9	96.5
GW-125	106.3	217.3	226.2	226.4	236.6	254.7	250.0	253.7	286.4	97.9
GW-129	98.0	220.9	230.0	229.0	239.1	258.2	252.8	256.2	290.2	90.5
GW-130	98.3	221.1	230.2	229.2	239.3	258.4	253.0	256.4	290.3	91.0
GW-131	80.6	224.8	234.1	232.0	241.8	262.1	255.9	259.0	294.3	105.3
GW-144	104.8	233.8	243.8	238.7	248.1	271.1	263.1	265.3	303.9	70.3
Mombacho South Side										
GW-181	106.7	258.8	270.6	257.0	265.0	295.9	282.5	282.4	330.3	42.2
Apoyo Lagoon area										
MW59	100.8	89.0	91.2	122.6	138.3	124.1	140.2	153.7	152.9	73.0
MW71	82.8	80.3	82.1	115.1	131.0	115.1	132.2	146.2	144.3	72.3
MW78	104.6	138.9	143.2	164.7	178.6	175.5	184.6	194.8	203.6	118.9
GW-83	114.6	89.3	91.5	122.9	138.6	124.5	140.5	154.0	153.2	173.6
GW-100	82.6	80.5	82.3	115.2	131.1	115.3	132.3	146.3	144.4	109.1
GW-103	69.3	169.4	175.4	189.3	202.0	206.5	210.7	218.5	235.6	108.2
GW-113	105.3	158.0	163.3	180.2	193.4	194.9	201.1	209.8	223.6	99.0
GW-119	104.5	139.3	143.7	165.0	179.0	175.9	185.0	195.1	204.0	95.2
GW-121	116.2	245.4	256.2	247.3	256.0	282.7	272.2	273.3	316.2	289.6
GWI5	176.3	197.7	205.3	211.4	222.7	235.1	234.2	239.6	265.6	102.5

TABLE 7: Gas geothermometry for Mombacho Volcano Region (ºC)

ID	utm-E	utm-N	D'Amore and Panichi gas geothermometer (ºC)
GG1	611.8	1307.5	N/A
GG2	611.7	1307.9	395
GW35	611.7	1307.9	394

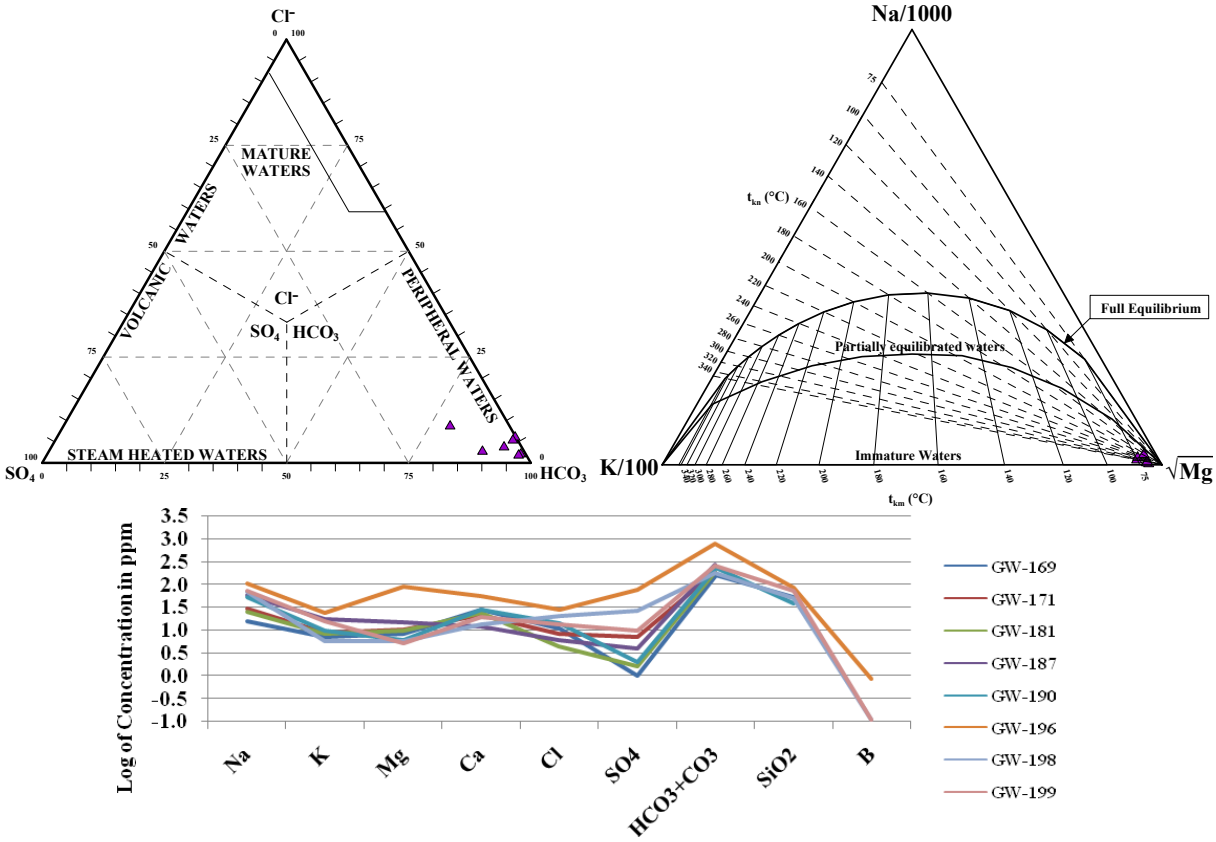

FIGURE 1: Ternary diagrams and Schoeller diagram for Masaya water samples

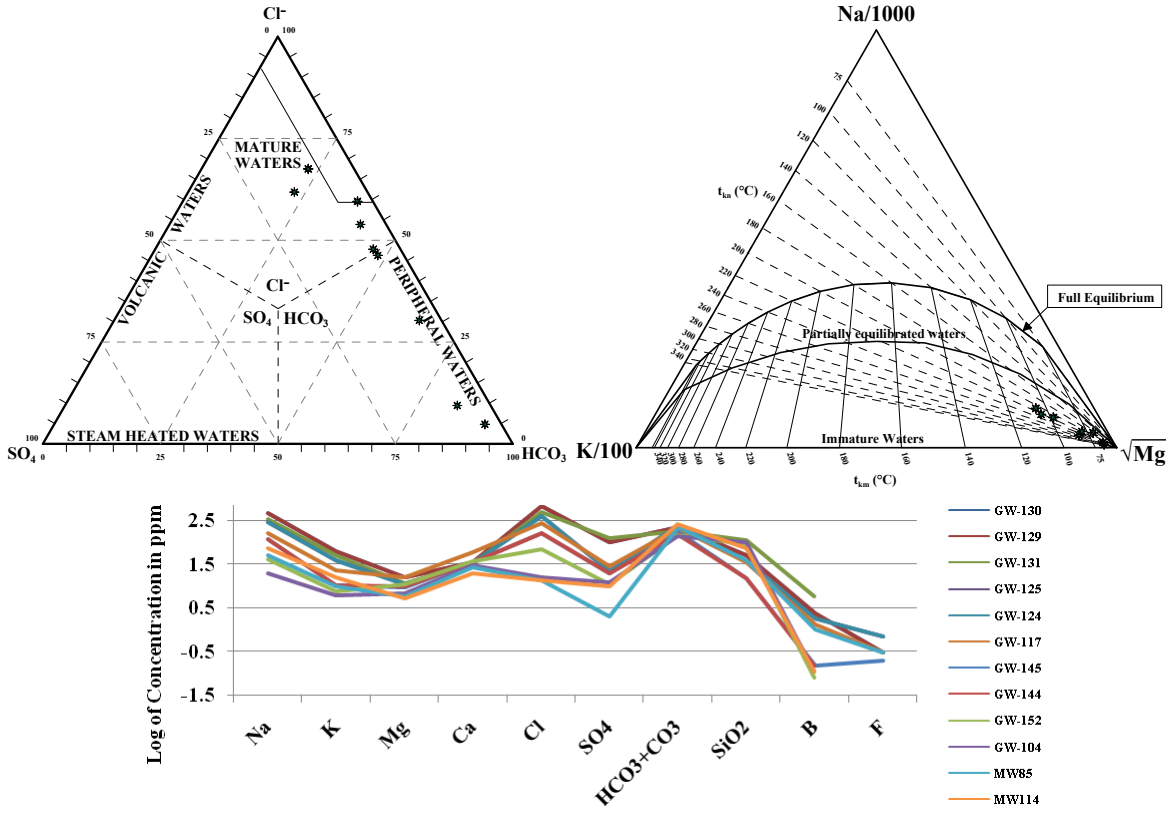

FIGURE 2: Ternary diagrams and Schoeller diagram for Granada City water samples

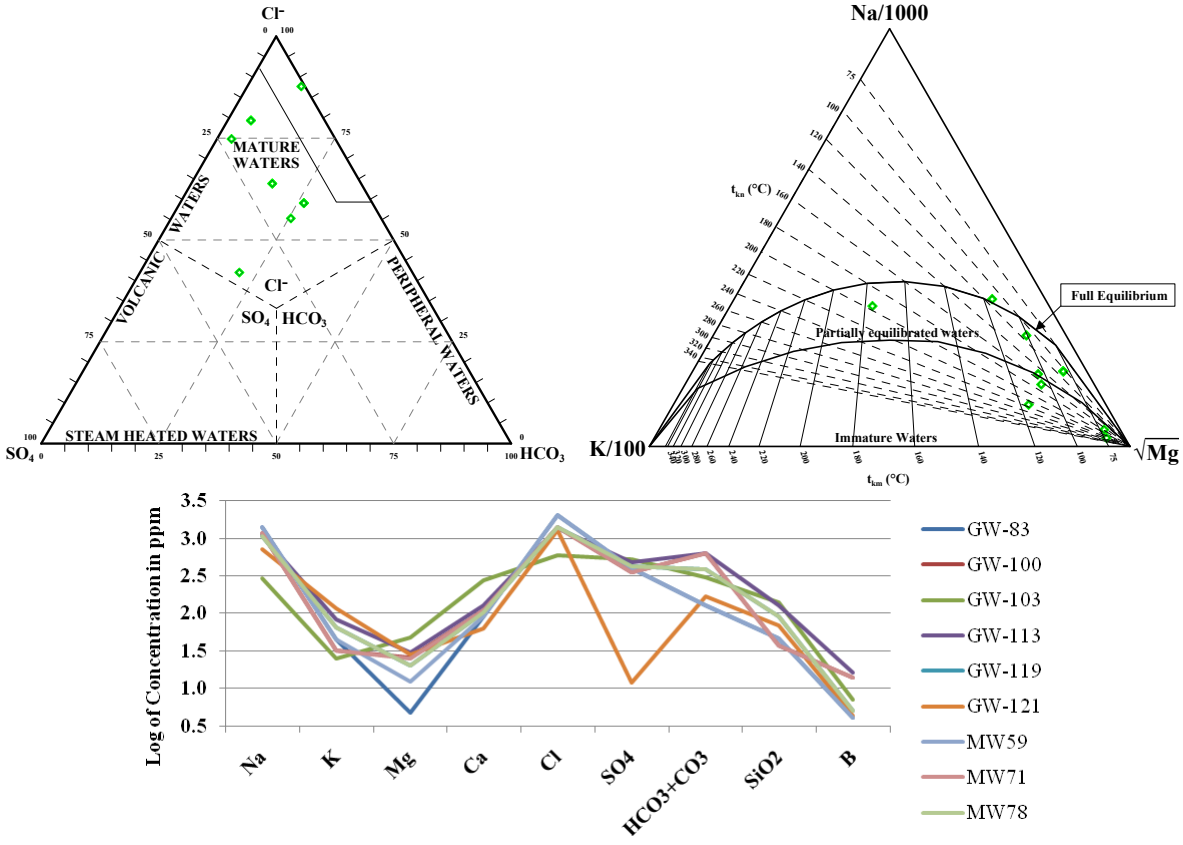

FIGURE 3: Ternary diagrams and Schoeller diagram for Apoyo Lagoon water samples

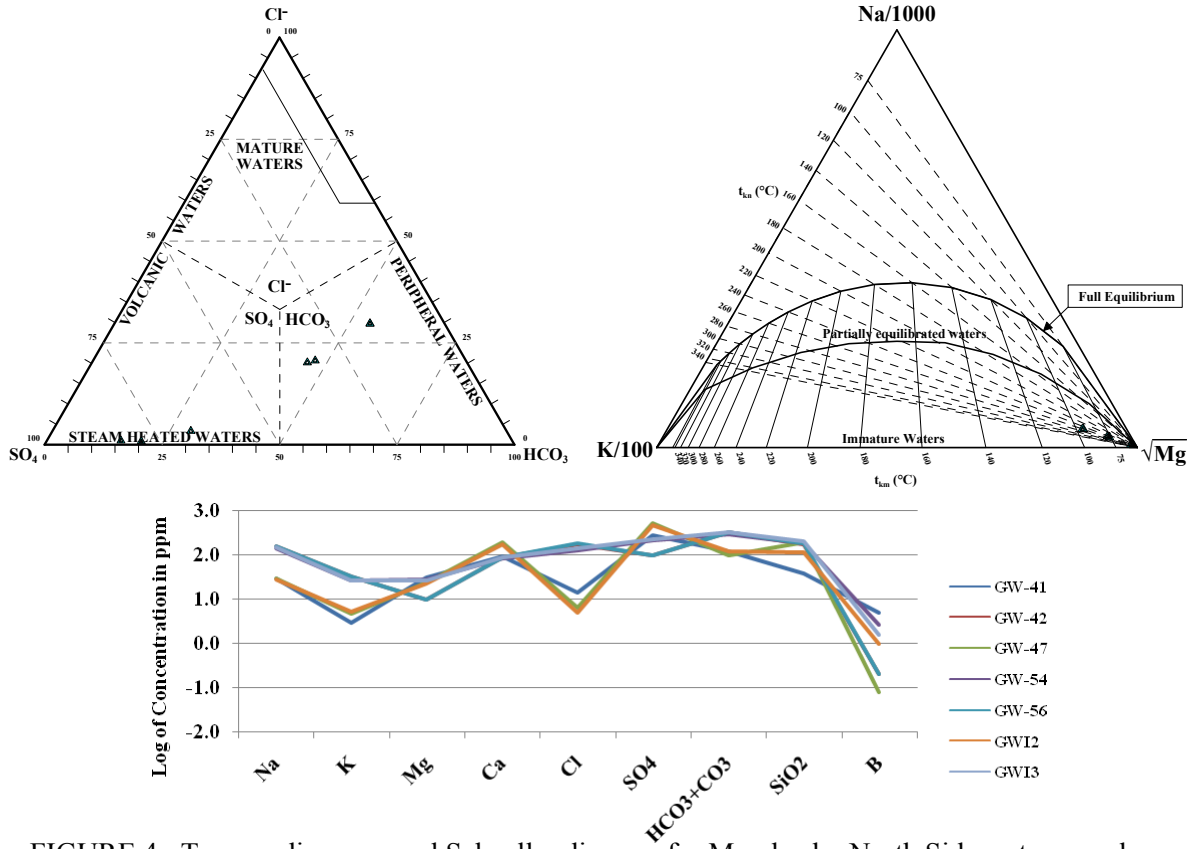

FIGURE 4: Ternary diagrams and Schoeller diagram for Mombacho North Side water samples

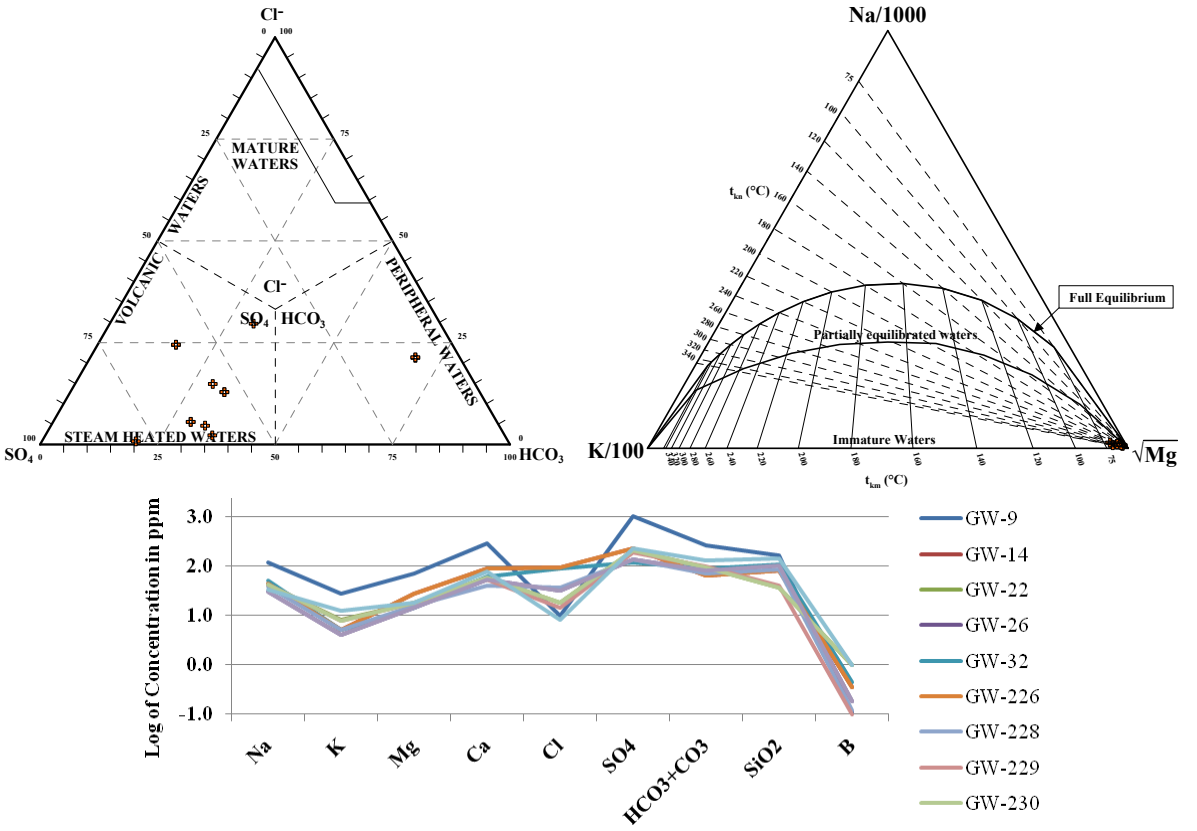

FIGURE 5: Ternary diagrams and Schoeller diagram of Mombacho volcano water samples

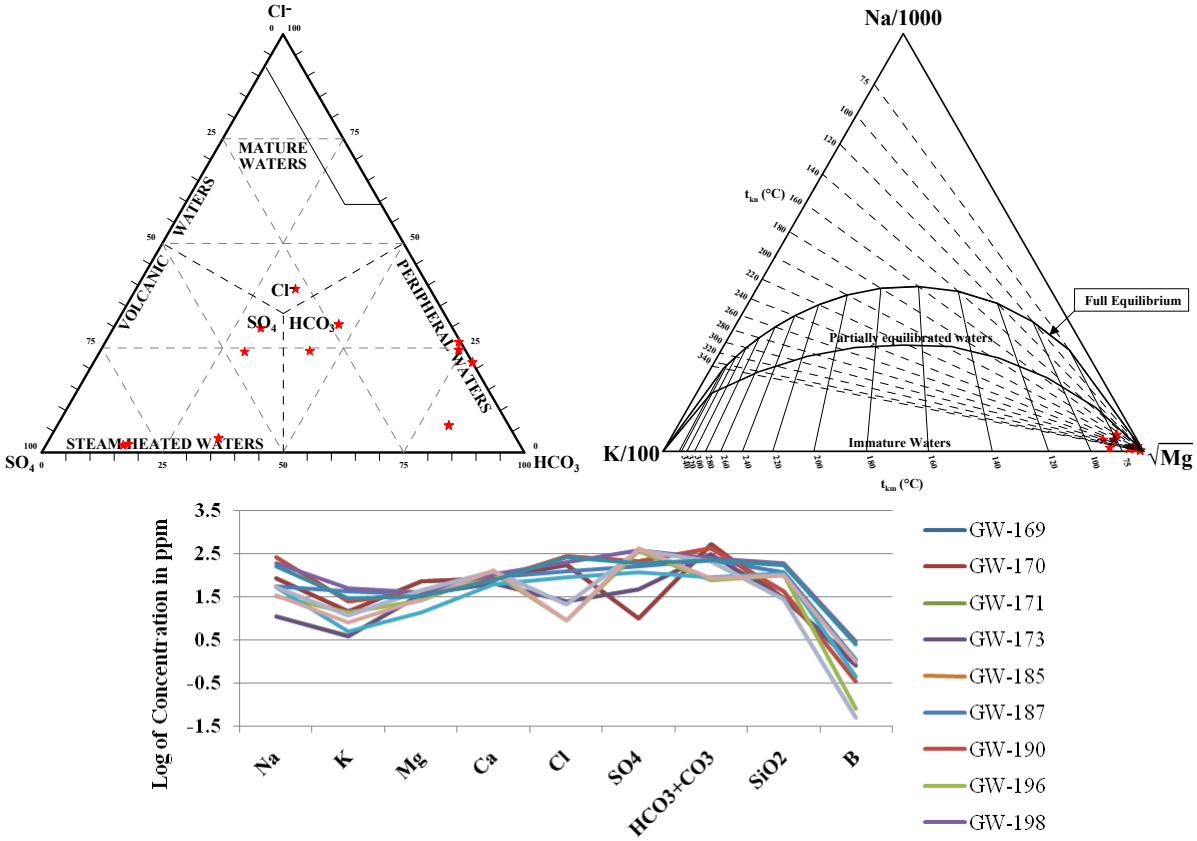

FIGURE 6: Ternary diagrams and Schoeller diagram of Mombacho South Side water samples

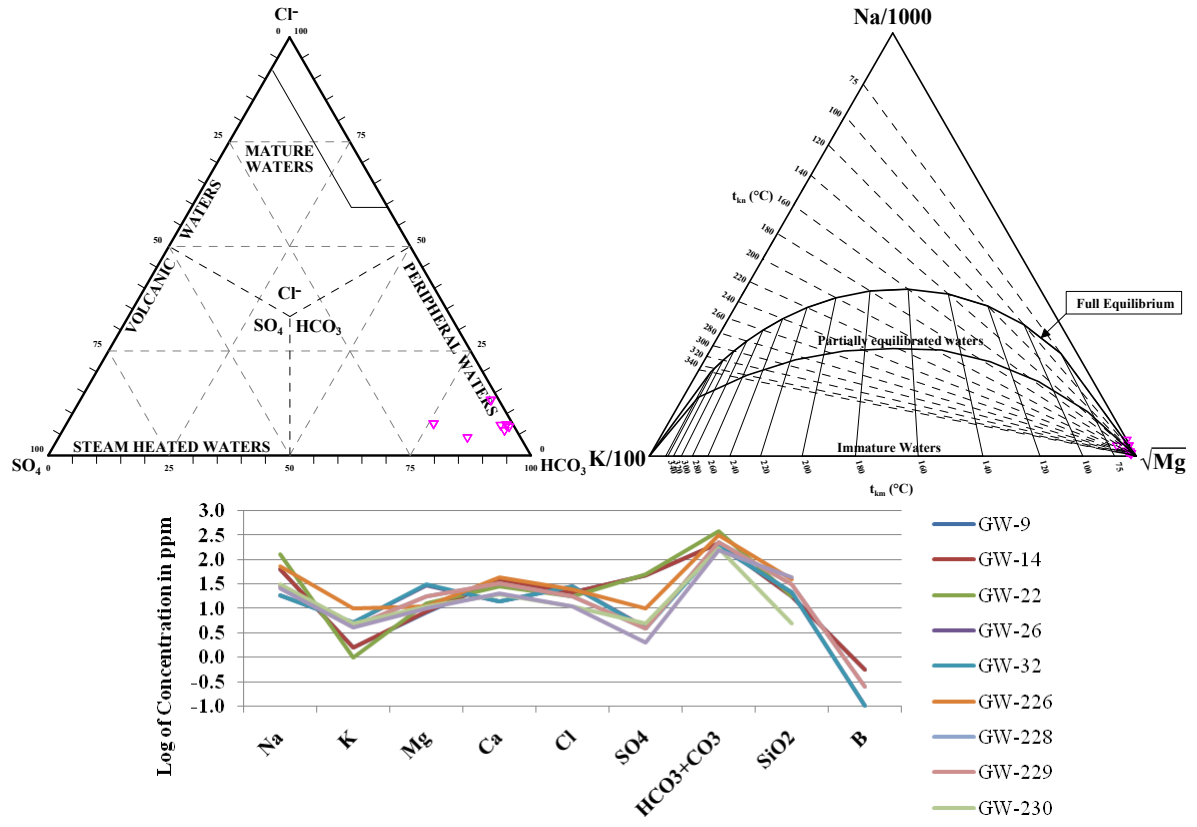

FIGURE 7: Ternary diagrams and Schoeller diagram of Nandaime water samples